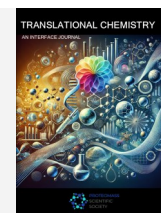




TRANSLATIONAL CHEMISTRY

AN INTERFACE JOURNAL

[HTTPS://WWW.TRANSLATIONALCHEMISTRY.COM/](https://www.translationalchemistry.com/)



REVIEW ARTICLE | DOI: 10.5584/translationalchemistry.v1i2.247

Colloidal Metallic Nanoparticles: An Introduction to Concepts and Properties

Silvia Nuti^{1,†,*}, Carlos Lodeiro^{1,2,*}

¹BIOSCOPE Research Group, LAQV-REQUIMTE, Chemistry Department, NOVA School of Science and Technology (FCT NOVA), Universidade NOVA de Lisboa, 2829-516 Caparica, Portugal. ² PROTEOMASS Scientific Society, 2825-466, Costa da Caparica, Portugal. [†] Current address: Department of Chemistry “Giacomo Ciamician”, University of Bologna, Via Gobetti 85, 40129 Bologna, Italy.

Received: 11 November 2025 **Accepted:** 22 November 2025 **Available Online:** 5 December 2025

ABSTRACT

Metallic nanoparticles (NPs) exhibit size- and shape-dependent properties that have positioned them at the forefront of nanoscience and nanotechnology. Their synthesis spans top-down and bottom-up approaches, including direct, seed-mediated, and composite strategies, each offering distinct advantages and limitations. Understanding nucleation, growth, and stabilization processes is essential to control morphology and functionality, which in turn govern their optical, catalytic, and biological behaviours. This introductory review provides a didactic overview of metallic NPs synthesis, highlighting the connection between structure and properties. Integrating historical context, theoretical principles, and practical examples, this review outlines the key concepts linking the synthesis, structure, and behaviour of metallic NPs.

Keywords: Noble metals, Nanoparticles, Synthesis, Colloids, Didactic

1. Introduction and historical perspective

Metals, such as Gold (Au), Silver (Ag), Platinum (Pt), Copper (Cu), have been used since antiquity, when they were prized for their ornamental and economic value and for their supposed healing powers [1–4]. When these materials are brought to the nanoscale range (10^{-9} m), they form structures called NP (from Ancient Greek “*vāvoc*” (nānos), meaning “*dwarf*”) which exhibit different properties when compared to the bulk metals, the most evident and captivating change is seen in the variation of the colour. Throughout history, several examples of the use of nanomaterials are reported. Cu and Ag nanocrystals were found in glazed pottery created by artisans in the Middle East in the 9th century [5]. Soluble Au was believed to have impressive curative properties, and its preparation and applications are described in two books dating back to 1618 and 1676 [6,7]. Au and Ag NPs of different sizes are the origin of the astonishing stained glass works: firstly developed in Ancient Egypt and Ancient Rome, the peak of the stained-glass windows creation was reached during the Middle Ages in the 12th century [8,9]. However, the finest example of the use of nanomaterials in antiquity is represented by the Lycurgus cup, a Roman cage cup-type vessel dating back to 4th century. Due to the presence of Au-Ag alloyed NPs, it exhibits different colour

depending on the illumination (**Figure 1**): when it is illuminated from outside, and light is reflected, it appears green, while, when it is illuminated from the inside, and the light is transmitted, the cup displays a red colour [10].



Figure 1. Lycurgus Cup (British Museum, London). When viewed in reflected light, it appears green (A). However, when the light is transmitted through the glass, it appears red (B). © The Trustees of the British Museum. Shared under a Creative Commons Attribution-NonCommercial-ShareAlike 4.0 International (CC BY-NC-SA 4.0) licence.

It was in 1857 that the observation of metallic NPs was described by the English scientist Michael Faraday in his Bakerian Lecture [11]. He was, in fact, able to obtain a ruby coloured solution and described how the colour was produced by fine particles of Au

*Corresponding author: Silvia Nuti, silvia.nuti3@unibo.it; s.nuti@campus.fct.unl.pt | Carlos Lodeiro, cle@fct.unl.pt

which are “very minute in their dimensions”, even though he could not observe them with the microscopes available at the time [12]. Almost one hundred years later, in 1951, John Turkevich and his colleagues observed the Au colloids with an electron microscope [13]. Faraday also noted that “the particles are easily rendered evident, by gathering the rays of the sun (or a lamp) into a cone by a lens, and sending the part of the cone near the focus into the fluid; the cone becomes visible, and though the illuminated particles cannot be distinguished because of their minuteness, yet the light they reflect is golden in character, and seen to be abundant in proportion to the quantity of solid gold present.”[11] observing the so-called Tyndall effect, also extensively studied in the same time frame by the Irish physicist John Tyndall.

Later on, in 1908, another important contribution to the growth of nanotechnology came from the German physicist Gustav Mie [14]. Mie theory is based on solving Maxwell's equations for electromagnetic waves interacting with a spherical particle. It describes the scattering and absorption of light by spherical particles whose size is comparable to or larger than the wavelength of the incident light and as NPs dimensions often fall within this range, the theory is particularly useful for their study. The interest towards nanotechnology and the synthesis of NPs with different composition, morphology and applications has increased significantly with a huge and constantly increasing number of documents published on this topic.

2. Synthesis of Metallic NPs

The synthesis of NPs holds immense importance in various fields of science and technology. The controlled synthesis of NPs enables researchers to tailor their size, shape, composition, and surface properties, allowing for precise manipulation of their characteristics and functionalities. Metallic NPs, with their unique physical and chemical properties, offer important opportunities for advancements in different areas such as medicine, electronics, energy, and environmental remediation.

2.1. Top-down and bottom-up approaches

The approaches for synthesising metallic NPs can be divided in two greater categories: “*top-down*” and “*bottom-up*” [15,16]. “*Top-down*” synthesis is based on the reduction of bulk materials, such as larger particles or bulk powders, to NPs through controlled mechanical, physical or chemical processes. Some of the most commonly used techniques are ball milling, mechanochemical synthesis, sputtering or laser ablation, where external forces are applied to reduce the size of the material or to induce reactions at the surface of the bulk reagents. On the other hand, “*Bottom-up*” synthesis focuses on building NPs from atomic or molecular precursors, gradually assembling them into the desired nanostructures. This approach includes many techniques in solid state (physical vapor deposition or chemical vapor deposition), liquid state (sol gel methods, chemical reduction, hydrothermal method, solvothermal method), gas phase (spray pyrolysis, laser ablation, flame pyrolysis) and other methods including biological synthesis, microwave or ultrasound techniques. One of the most

common methodologies among the “*bottom-up*” approaches is the chemical reduction method or also called wet colloidal synthesis, in which NPs are synthesized by controlling chemical reactions in a solution. This process evolves through two different phases: nucleation and growth.

2.2. Nucleation and Growth of Metallic NPs in Solution

The nucleation and growth processes are the steps involved in the colloidal synthesis of metallic NPs [17,18].

2.2.1. Nucleation

Nucleation is a thermodynamic step that leads to the formation of tiny clusters (or nuclei) from precursor species in solution. This can be initiated by, for example, the addition of a reducing agent or temperature variations. Nucleation can be distinguished by the way it occurs:

- *Heterogeneous nucleation* occurs at preferential sites such as, phase boundaries, impurities or surfaces or particles present in the system that act as nucleation sites and typically requires a lower amount of energy to be initiated.
- *Homogeneous nucleation* occurs when nuclei form spontaneously in the reaction solution. It requires a higher amount of energy together with other conditions such as supersaturation.

Nucleation is mainly explained by the Classical Nucleation Theory (CNT) [19] in which, for a spherical particle of radius r , the total free energy ΔG , is given by the sum of the surface energy γ and the free energy of the bulk crystal ΔG_v (Equation 1):

$$\Delta G = 4\pi r^2 \gamma + \frac{4}{3}\pi r^3 \Delta G_v \quad (1)$$

The free energy of the crystal, ΔG_v (Equation 2), is governed by parameters such as temperature (T), Boltzmann's constant (k_B), the supersaturation of the solution (S) and its molar volume (v) (Equation 3).

$$\Delta G_v = \frac{-k_B T \ln(S)}{v} \quad (2)$$

$$S = \frac{C_{\text{actual}} - C_{\text{equilibrium}}}{C_{\text{equilibrium}}} \quad (3)$$

Because the surface free energy is positive while the crystal free energy is negative, it is possible to find a maximum free energy corresponding to a critical cluster size. The critical radius of the nucleus identifies to the minimum size required for a particle to persist in the solution without undergoing re-dissolution. Conversely, when clusters exceed the critical radius r , growth becomes favourable (**Figure 2**). The critical radius is expressed as follows in Equation 4:

$$r_{\text{crit}} = -\frac{2\gamma}{\Delta G_v} \quad (4)$$

By substituting r in Equation 1 with critical radius from Equation 4 it is possible to obtain the expression for the critical free energy ΔG_c (Equation 5):

$$\Delta G_{\text{crit}} = \frac{16\pi\gamma^3}{\Delta G_v^2} \quad (5)$$

Consequently, nucleation can be promoted by increasing the supersaturation level, resulting in a reduction of the energy barrier for nucleation and raising the temperature, which increases the average atomic energy and facilitates the overcoming of critical energy or by introducing a change in surface free energy, achievable through the use of surfactants.

2.2.2. Growth

Different theories have been proposed to describe the growth of NPs following nucleation. Some theories explain the growth of NPs as atom-mediated while other as NPs-mediated. In the former, the atoms act as building blocks that aggregate on the surface of a growing nucleus, contributing to its expansion, while the latter theory involves the addition of pre-existing NPs as the fundamental units for further growth. The most representative theories are summarized below:

- *LaMer* mechanism was one of the first nucleation and growth theory to be proposed and is based on the CNT [20]. Developed for a closed system, this model describes the formation of NPs in three stages: first, an increase in the concentration of available monomers within the solution which initiates the second stage, a phenomenon called "burst nucleation," resulting in a substantial decrease of free monomers in the solution (Figure 3). The nucleation rate during this phase is characterized as "effectively infinite", causing minimal nucleation activity thereafter due to the diminished concentration of monomers, lastly growth continues controlled by the diffusion of monomers through the solution.
- *Ostwald and digestive ripening* are mechanisms that propose to explain the growth of NPs in solution. Ostwald ripening [21] (Figure 4A) occurs due to differences in solubility and surface energy between larger and smaller particles. Larger particles have

lower surface energy and are more thermodynamically stable, leading to the preferential dissolution of smaller particles and subsequent growth of larger ones. On the other hand, digestive ripening [22] (Figure 4B) happens when bigger NPs dissolve and the smaller ones grow. Digestive ripening can be initiated with the addition of a ligand that will help the dissolution of the bigger particles. With the equilibrium of the two process a more uniform size distribution is achieved.

- *Coalescence and Oriented attachment* are two mechanisms that explain the growth of nanocrystals as "nanoparticle-mediated growth", that occurs when smaller NPs, created in the initial stages of the reaction, merge to create bigger NPs. For *coalescence* [23] (Figure 5) there is no preferred merging site for the NPs that will coalesce upon contact. Conversely, for *oriented attachment* [24] (Figure 6) to happen, the NPs must present matching crystallographic planes. This mechanism might occur following collisions of aligned nanocrystals in suspension or when misaligned NPs will rotate towards a low-energy interface configuration.

2.3. Stability of NPs

Once NPs are synthesised, their stability in solution refers to the ability of colloidal particles to remain dispersed in a medium without aggregating or settling over time. Stability of NPs is crucial for maintaining their properties and it is also important for their further application. Multiple parameters govern colloidal stability, including van der Waals (vdW) attraction, electrostatic double-layer (EDL) repulsion, particle-size distribution, pH, temperature, surface chemistry, and steric effects [25]. vdW attractive forces (Figure 7A) result from the interaction of induced, instantaneous or permanent dipoles in between NPs and tend to destabilize the colloidal dispersion. These attractive forces are counteracted by electrostatic repulsion generated by the NPs EDL (Figure 7B).

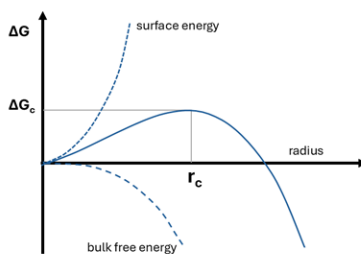


Figure 2. The dependence of the cluster free energy, on the cluster radius, according to the CNT.

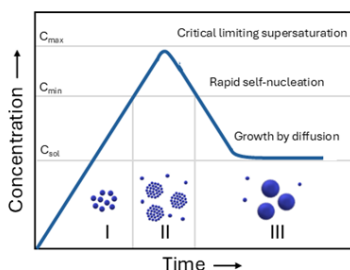


Figure 3. The principle of nanoparticle nucleation due to LaMer's mechanism of nucleation derived from CNT.

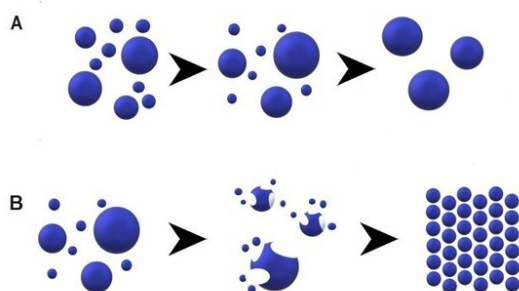


Figure 4. Representation of the (A) Ostwald ripening and (B) digestive ripening processes.

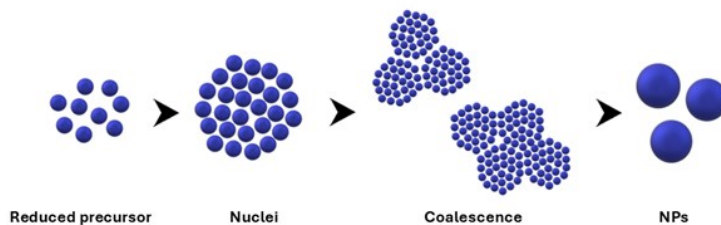


Figure 5. Representation of coalescence in the synthesis of NPs.

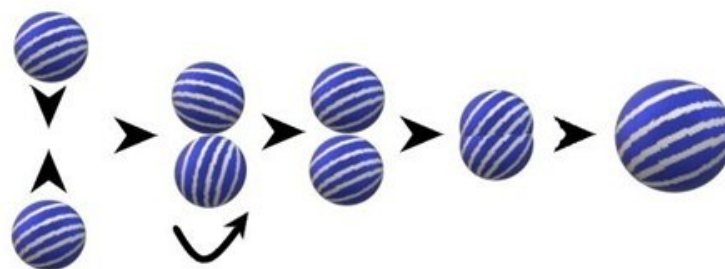


Figure 6. Representation of an oriented attached mechanism.

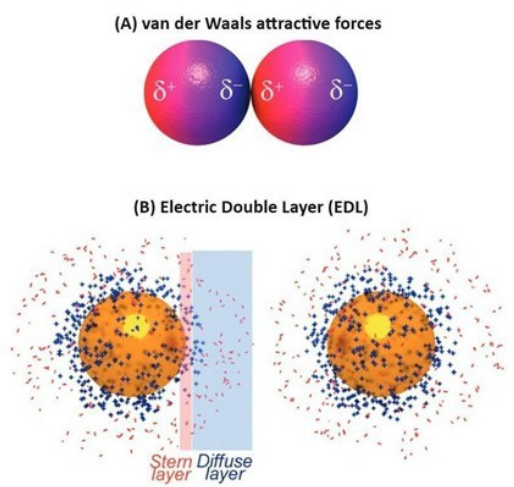


Figure 7. (A) Representation of Van der Waals interactions that can lead to nanoparticle aggregation. (B) Representation of the EDL, composed by the Stern layer and the Diffuse layer. Adapted with permission from reference [25]. Copyright 2015 Royal Society of Chemistry under a CC BY 3.0 License <https://creativecommons.org/licenses/by/3.0/>.

The EDL is formed by the Stern-layer and the diffuse layer. The surface charge of NPs, originating from surface ions or functional groups, leads to the creation of the Stern layer formed by ions with opposite charges adhering to the NP surface. The diffuse layer is formed by ions carrying a charge opposite to that of the Stern layer. The EDL results in a net charge, and when two similar particles are in proximity, the EDL causes repulsion between them. The Derjaguin–Landau–Verwey–Overbeek (DLVO) theory uses vdW forces and EDL to predict and explain NPs stability. The DLVO theory also includes contribution of pH and ionic strength of the medium. Steric stabilization (**Figure 8**), obtained through the adhesion of molecules (polymers, proteins, surfactants...) to the NPs surface, becomes a valuable tool in maintaining the dispersion of NPs, especially in challenging conditions, as it prevents the formation of attractive vdW interactions between two particles. The stability is now determined by the solubility of the molecules, average chain length, concentration or temperature. Steric stabilization will be ineffective if the obtained coating is patchy or incomplete.

2.4. Direct synthesis

Direct synthesis (also known as "one-pot") is the most straightforward method to synthesise metallic NPs in solution. This approach combines nucleation and growth happening simultaneously and in the same vessel. The metal precursor is reduced, and the newly formed NPs need to be stabilized by a capping agent present in the solution. One of the most commonly reproduced one-pot syntheses is the Turkevich synthesis. Firstly reported in 1951 [13], it involves the use of tetrachloroauric(III) acid (HAuCl_4), which is reduced and stabilized by trisodium citrate at 100 °C in water, for the preparation of spherical Au NPs with a diameter of approximately 20 nm.

Early reports of one-pot synthesis of Ag NPs, where the reduction of the metal precursor (AgNO_3) is achieved using sodium borohydride (NaBH_4) showed a less uniform size and shape distribution [26]. More recently, the one-pot synthesis of monodisperse Ag NPs, of approximately 10nm, was reported [27]. This methodology utilizes a combination of sodium citrate and tannic acid as reducing agents for AgNO_3 . It is also possible to obtain Pt NPs via a one-pot methodology [28]. In this case the reduction of the metal precursor, hexachloroplatinic acid (H_2PtCl_6) is achieved with a combination of acetylthiocholine (ATC) and NaBH_4 . While direct synthesis methodologies are popular due to their simplicity, they often lead to NPs with a spherical morphology, thus, to obtain a higher degree of control over

morphology and sizes of NPs it is necessary to resort to seed-mediate syntheses.

2.5. Seed-mediated synthesis

In seed-mediated syntheses methodologies, pre-formed particles are used as "seeds" and act as nucleation sites for the formation of the desired NPs. Typically, this methodology allows for a finer tuning of the NPs size and morphology. One of the first reported examples is the synthesis of Au nanorods [29] starting from pre-formed Au spherical seeds and utilizing cetyltrimethylammonium bromide (CTAB) as a surfactant for the formation of the rod-shaped NPs. Shortly after, the synthesis of Ag nanowires using pre-formed Pt seeds and a polyol process, was reported [30]. This approach is also applicable to spherical NPs. Starting from seeds obtained with a one-pot methodology, researchers have been able to grow Ag and Au spherical NPs [27,31] with a great control over their size distribution. Proceeding after the first step, and using the previously grown NPs as seeds, the process has been extended to several NPs generations obtaining spheres up to 200 nm. However, a greater understanding of the nature of the seeds and an appropriate choice of capping agents and surfactants, can lead to the synthesis of a broader variety of morphologies [32].

A seed can be characterized by two elements: the internal structure (or crystallinity) defined by planar defects such twin planes or stacking faults, and the surface structure (or faceting). Most noble metals crystallize in the face centred cubic (fcc) lattice, which can be explained as the stacking of closely packed, hexagonal arrays of atoms along the (111) direction.

- *Single-crystal seeds* do not present any planar defects and consists of only one single-crystal domain. They can be obtained when a strong reducing agent is used for their preparation.
- *Singly twinned seeds* present one planar defect, a (111) plane that serves as a twin boundary dividing the seed in two crystal domains. Metals such as Cu, Ag, Au often produce this type of seeds.
- *Multiply twinned seeds* are characterized by the presence of more than one twin defect. This type of seeds can be helpful in the synthesis of highly anisotropic NPs, thanks to the inhomogeneous distribution of the defects.
- *Plate-like seeds* are generated when stacking fault defects are present. The synthesis of this type of seeds is more intricate, due to the necessity of having a kinetic control over the growth of the NPs. Slow deposition of the atoms, use of mild reducing agents and the use of strong ligands are some of the favoured strategies [32].

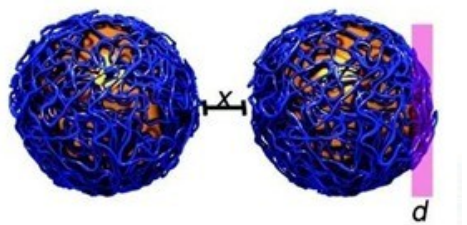


Figure 8. Representation of NPs covered with a polymer avoiding particle interaction due to steric repulsion. Adapted with permission from reference [25]. Copyright 2015 Royal Society of Chemistry under a CC BY 3.0 License <https://creativecommons.org/licenses/by/3.0/>.

Capping agents also influence the homogeneous nucleation over a pre-formed seed. Some molecules bind strongly to certain metals while other have a weaker interaction (for example, citrate will weakly bind to Au, while thiols will have a much stronger interaction). The combination between the affinity of a capping agent for a metal/specific facet will have an influence on the growth of the final NPs, as a facet that is selectively capped will be more expressed during the growth [32].

Seed-mediated protocols provide a wide range of potential morphologies beyond the nanorods and spheres mentioned earlier. Additional morphologies achievable through seed-mediated syntheses include nanoplates [33], nanocages or nanoframes [34], and branched NPs (also referred to as nanostars, nanoflowers, multipods or dendritic NPs, based on the branches number and distribution) [35]. Nanoplates represent an important class of anisotropic nanostructures distinguished by their pseudo-two-dimensional morphology with large lateral dimensions compared to thickness. One of the earliest reported examples is photoinduced method for the conversion of Ag nanospheres into triangular nanoprisms. In this process, light irradiation induces the fragmentation of spherical Ag NPs into small clusters that contribute to the growth of nanoprisms, acting as seeds, until all precursors are consumed. [36]. Around the same period truncated Ag nanoplates have been prepared through a soft-template approach using CTAB micelles [37] while PVP-assisted syntheses enabled the formation of nanoplates of other metals such as Au and Pd [37]. The formation of these plate-like structures has been associated with the presence of planar twin defects along the (111) crystallographic planes, which break the symmetry of the face-centred cubic lattice and promote two-dimensional growth. Additionally, selective ligand adsorption on specific crystal facets stabilizes the basal planes and restricts growth along the perpendicular direction, further favouring the plate morphology. One of the most striking features of this materials, when synthesised with plasmonic metals such as Au and Ag, is the possibility of tuning the LSPR band over an extensive range, from the visible to the infrared, by tuning the aspect ratio of the nanoplates by changing the synthesis conditions [38–40], making them ideal candidates for sensing applications [39].

Nanocages are a unique class of hollow nanostructures characterized by high surface-to-volume ratio, accessible inner cavities, internal and external surfaces and porous walls. They are most commonly synthesized through galvanic replacement reactions, where a less noble metal is oxidized and dissolved while a more noble metal is reduced and deposited onto its surface. In one of the first reported examples [41] Ag nanostructures were used as templates and reacted with HAuCl_4 , where Ag was oxidized to Ag^+ while Au^{3+} was reduced and deposited on the template surface, forming hollow Au shells after the complete consumption of Ag. The morphology, wall thickness, and void size of the resulting hollow structures were dictated by the size and shape of the Ag templates. This methodology was later extended to other noble metals, such as Pt and Pd, to further demonstrate the potential of this approach which was subsequently adopted for the synthesis of [42] both single- and double-shell nanocages (Au-Pt, Pt-Au, Au-Pd, Pd-Au, Pd-Pt, and Pt-Pd) via sequential galvanic replacement

steps. The optical and plasmonic characteristics of these hollow nanocages were found to depend strongly on the dielectric properties and shell thicknesses of the constituent metals. More recently, a seed-mediated method combining Pd nanocube templates, Pt-Ru deposition, and subsequent chemical etching to obtain multimetallic PdPtRu nanocages was reported [43]. The resulting nanocages exhibited open, hollow structures with tunable compositions and demonstrated significantly enhanced catalytic activity and durability. Overall, galvanic replacement and related template-mediated strategies have proven to be powerful synthetic routes for producing nanocages with controllable morphology, wall thickness, and composition. These advances have established nanocages as versatile materials for applications in catalysis, plasmonics, and energy conversion.

Branched NPs have been obtained with different metal precursors. Ag nanoflowers have been obtained from the reduction of $[\text{Ag}(\text{NH}_3)_2]^+$ by ascorbic acid, in the presence, polyvinylpyrrolidone (PVP) as stabilizer, trisodium citrate and employing single crystalline silver seeds [44]. Pd nanostars were obtained using a two-step seeded growth process, using PdCl_4^{2-} as precursor, ascorbic acid as reducing agent, CTAB as stabilizer, and copper (II) acetate to promote the anisotropic growth of different morphologies depending on its concentration [45]. For Pt, different methodologies have been reported, either using Pt seeds [46] in presence of PVP to produce single crystal NPs or Au seeds [47] to catalyse the thermal decomposition of PtCl_2 in oleylamine. Rh multipods have been prepared with the reduction of RhCl_3 in ethylene glycol in presence of PVP using Rh seeds [48].

Great research effort has been dedicated to creating branched Au NPs, thanks to their intense and highly tunable Localized surface plasmon resonance band (LSPR), enabling applications in different fields [49]. One of the first reports of Au branched NPs involved the use of PVP in dimethylformamide (DMF) both as reducing and stabilizing agent and PVP coated seeds [50]. Following the first reports on the role of AgNO_3 as shape inducing agent for the synthesis of Au nanorods [51,52], a similar methodology has been applied for the synthesis of branched Au NPs in combination with the use of surfactants such as CTAB [53,54]. The use of branched NPs in sensing and biomedical applications has been limited by the potential toxicity of surfactants like CTAB, and by the difficulty of replacing the stabilizing agents (i.e: PVP, CTAB), for further functionalization. Surfactant-free synthesis can help to advance in the bioapplication of branched NPs. Such syntheses are for example obtained with sodium citrate and hydroquinone, ascorbic acid or albumin [55–57]. Anisotropic metal NPs represent a highly versatile class of nanostructures whose design has evolved from spheres and rods to more complex morphologies such as nanoplates, nanostars, nanocages, multipods, and chiral or hierarchical architectures. The emergence of such complex architectures further illustrates the structural diversity attainable through colloidal synthesis. The ability to modulate shapes and composition at the nanoscale enables fine control of optical, catalytic, and electronic responses, supporting applications that span from SERS and chemical sensing to photocatalysis, photothermal therapy, and energy conversion [58].

2.6. Synthesis of Composite NPs

Composite NPs possess a structure comprising two or more components at the nanoscale, each exhibiting distinct physical and/or chemical properties. These components possess mutual contact interfaces, leading to a strong coupling effect on a nanometer scale. Composite NPs can combine the effects of individual components or enhance intrinsic performance and exhibit novel features, surpassing the limitations of single-component properties. Examples of composite NPs studied in this thesis work include bimetallic NPs in core@shell or alloyed morphology and metal@oxide core@shell NPs such as metallic NPs with a bulk or mesoporous silica (SiO_2) shell.

2.6.1. Bimetallic NPs

Bimetallic NPs can be synthesised in solution with similar approaches compared to their mono-metallic counterparts (“*top-down*” or “*bottom-up*” approach and direct or seed-mediated syntheses). The presence of the two metallic precursors will determine the final composition of the particles [59]. For the “*bottom-up*” approach, if the two precursors are reduced simultaneously, it is likely that the NPs will present an alloyed structure (**Figure 9A**). The two metals might be present in a statistical mixture [60] or some zones of the particles might exhibit a richer composition of one of the two metals without complete segregation [61]. Conversely, if the second metal precursor is added to a pre-formed particle (like in a seed mediated synthesis) different outcomes are possible:

- **Formation of a core@shell structure:** In this case the second metal will be reduced on the surface of the NPs creating a shell that can be continuous or patchy (**Figure 9B**).
- **Formation of a hollow structure:** This process is also referred to as “galvanic replacement” and it consists of a redox process between the pre-formed metallic NPs (sacrificial template), and metal ions

in solution. The difference in the electrical reduction potential between the sacrificial template and the metal ions in solution provides the driving force for the reaction in which the template will undergo oxidation and dissolution while the second metal ions will reduce and deposit at the surface of the template. The resulting hollow NPs will have a composition richer in the second metal. Carefully tuning the relationship between the two metal can lead to different compositions of the hollow structures (**Figure 9C**) [62,63].

Bimetallic NPs can also be synthesised through “*top-down*” methodologies, an example of this is the laser ablation method in which a bulk alloy is irradiated with a laser to obtain bimetallic NPs (**Figure 9D**) [64–66]. With this methodology it is also possible to obtain ligand-free NPs [67].

2.6.2. Noble metal@oxide core@shell NPs

Controllable integration of different materials such as noble metals (Au, Ag, Pt, and Pd) and oxides (SiO_2 , TiO_2 , CeO_2 , Cu_2O , Fe_2O_3 , ZnO , SnO_2 and ZrO_2 [68–70]) into a single nanostructure has recently become a popular research topic as these nanostructures not only combine the function of individual NPs, but also bring unique collective and synergetic properties compared with single-component materials [71]. Moreover, an oxide shell can offer extra stabilization preventing the NPs aggregation or synergetic properties compared with single-component materials [71]. Moreover, an oxide shell can offer extra stabilization preventing the NPs aggregation or synergetic properties compared with single-component materials [71]. Moreover, an oxide shell can offer extra stabilization preventing the NPs aggregation or synergetic properties compared with single-component materials [71].

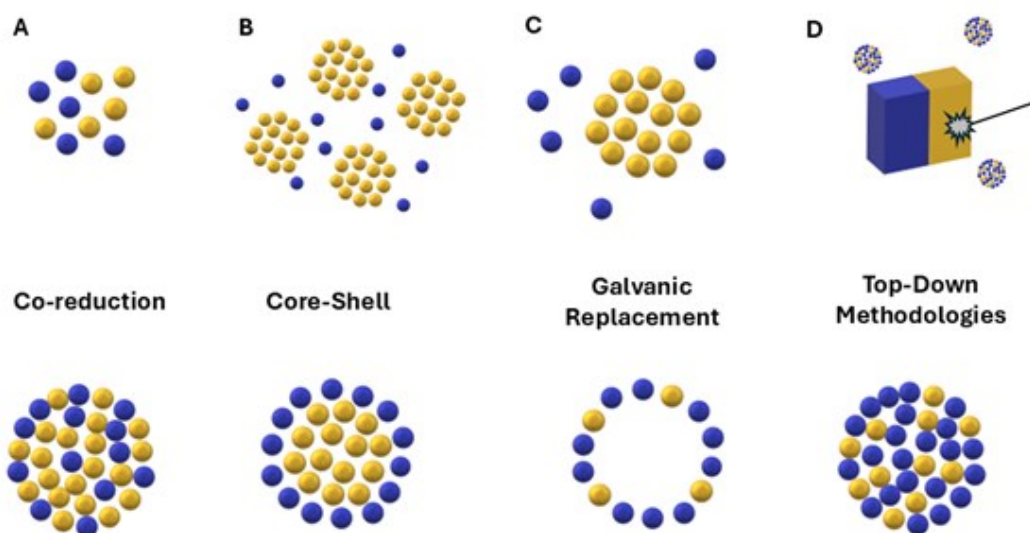


Figure 9. Schematic illustration of common synthetic strategies for bimetallic NPs. (A) Co-reduction: simultaneous reduction of two metal precursors yields alloyed NPs with a mixed atomic distribution. (B) Core-shell growth: sequential nucleation produces NPs where one metal forms the core and the second metal forms the shell. (C) Galvanic replacement: a sacrificial template undergoes partial dissolution, leading to hollow or porous bimetallic structures. (D) Top-down methodologies: bulk alloys are fragmented through processes such as laser ablation, sputtering, or ball milling.

Some of the first reports of these types of materials concerns the growth of Au-labeled SiO₂ particles [77] and a homogeneous SiO₂ shell on Au NPs [78]. These studies were motivated by the necessity of stabilizing the particles without hindering their properties and for this purpose SiO₂ has been proved to be an ideal candidate due to its inertness and transparency. Due to the scarce affinity of Au for SiO₂ (vitreophobic character), caused by the absence of the formation a superficial passivating oxide film in solution and to the presence of organic anions, the NPs had to undergo a functionalization step using aminopropyltrimethoxysilane (APTMS) to prime the surface for the following SiO₂ growth, making it vitreophilic. The SiO₂ growth was then promoted on the NPs acting as nucleation sites, applying the Stöber method via hydrolysis and condensation of tetraethylorthosilicate (TEOS, Si(OC₂H₅)₄) in an alcohol/water mixture [79]. This method had been also applied to the coating of Ag NPs [80] and the first test of this composite system in the catalysis of a redox reaction [81]. Moreover, both Au@SiO₂ and Ag@SiO₂ have been subjected to harsh condition to demonstrate core corrosion. This consequently demonstrates that the SiO₂ layer has an inherently porous character that allows for diffusion of metal ions and/or reagents through the pores [82]. These experiments demonstrated that the SiO₂ layer will not hinder the properties of the metallic core, thus paving the way for a series of applications of these nanocomposites. Further methodologies have been explored to prevent the dissolution of more sensitive cores, such as Ag, and to stabilize NPs before the SiO₂ coating synthesis such as the use of PVP [83], polyethylene glycol (PEG) [84], layer-by-layer (LbL) polyelectrolyte wrapping [85], use of surfactants [86], glucose [87]. To obtain composite nanomaterials with a greater variety of properties and possible applications is it also possible to synthesise a mesoporous silica coating. This type of material is characterized by the presence of ordered pores in between 2 nm and 50 nm in diameter. The first example of a tunable mesoporous silica structure (called MCM-41) (Figure 10) was obtained with the use of surfactants. These surfactants form micelles in the synthesis solution and the micelles form templates that create the mesoporous framework around which the silica precursor will condense to form the final structure. The template was then removed by calcination. For the MCM-41 synthesis the most used surfactant was CTAB [88]. Spherical Au NPs are among the first examples of metallic NPs individually coated with a mesoporous SiO₂ layer [89,90]. In the first reports, the NPs were subjected to the vitreophilization process [78], previously reported for amorphous SiO₂ coatings, and also were coated with a thin layer of dense SiO₂ before the mesoporous coating synthesis. A more direct approach for the mesoporous shell synthesis has been demonstrated on Au nanorods [91], in this process CTAB was used

as both NPs stabilizer and SiO₂ template, without the necessity of the intermediate vitreophilization step. Similarly, the precise control over the shell thickness was achieved by regulating the TEOS amount and addition rates and/or by stopping SiO₂ condensation with PEG-silane at the desired thickness [92]. Since then, different metals and their respective oxides have been encapsulated in a variety of mesoporous SiO₂ shells architectures leading to the application of these composite nanomaterials in a variety of fields (biomedicine, catalysis, sensing, gas storage) [93,94].

2.7. Biogenic synthesis of NPs

Biogenic synthesis of NPs, frequently referred to as "green synthesis," consists of group of methodologies for the synthesis of NPs with the use of naturally sourced molecules and organisms [95,96]. These methodologies can be categorized into two main groups:

- *Plant-mediated*: this group of syntheses includes intracellular and extracellular (plant extracts or extracted phytochemicals) processes. Some plants have the capability of accumulating metals and produce NPs thanks to the variety of molecules present in their structure. While various methodologies exist, the predominant approach involves the utilization of plant extracts. The extracts serve dual roles as reducers and potential stabilizers or capping agents. They are added to the solution containing the metal precursor and, thus, most methodologies are classifiable as "direct syntheses".
- *Microbial synthesis*: several microorganisms such as bacteria, fungi, algae, yeasts and viruses are also reported to synthesize metallic NPs. Depending on the type of microorganism the synthesis can happen intracellularly or extracellularly. The extracellular synthesis method is favoured for its straightforward and simpler purification steps. Conversely, the intracellular synthesis presents challenges and higher costs due to the necessity of additional separation and purification steps. The formation of NPs during the microbial synthesis process occurs through the oxidation/reduction of metallic ions by biomolecules secreted by microbial cells (enzymes, sugars, carbohydrates, proteins). Nonetheless, the microbial synthesis pathways are not yet completely understood due to the variation among the different microorganisms.

Biogenic synthesis of NPs offers clear advantages: it is eco-friendly and produces biocompatible NPs. Some of the synthesised NPs might retain biological activity deriving from the source material and can subsequently be applied in areas such as antimicrobial coatings, agricultural products, and environmental remediation [97,98].

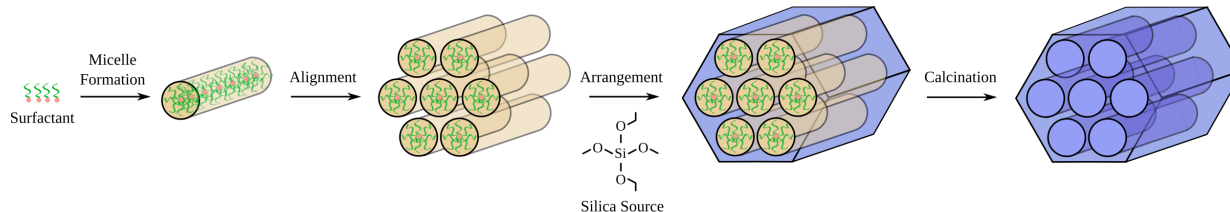


Figure 10. Synthesis pathway of MCM-41. Reproduced from Hermann Luyken - Own work, CC0, [wikimedia.org/w/index.php?curid=32258196](https://commons.wikimedia.org/w/index.php?curid=32258196).

On the other hand, these protocols might also present significant drawbacks. When using plants extracts, the availability of the plants, fruits, and flowers and the composition of their extracts might depend on seasonality, geography and growth conditions, which in turn affects reproducibility, scalability, and NPs purity [97]. The plants or their extract might also have to be preserved before their use, and this increases the energy cost of the process [99]. Similarly, microorganisms might have to be grown for the purpose of synthesis, adding a costly step, in terms of time and energy, to the process. Oftentimes, the NPs obtained with biogenic synthesis lack in monodispersity (size and shape) and stability making their application and scalability more challenging [100,101]. Nevertheless, advances in synthetic protocols continue to improve the morphology and monodispersity of biogenically produced NPs [102].

3. Optical Properties of Metallic NPs

'Metals' optical properties are governed by conduction electrons that move freely on the metal. An electromagnetic source can influence and drive the movement of these electrons. The electromagnetic source can induce an oscillation that resonates with the shape of the metal surface and in this case a surface plasmon resonance is generated [69,103,104].

At the macroscopic level, when an electromagnetic wave interacts with the metal, the electric field of the wave can cause the collective oscillation of the electrons, this phenomenon is known as surface plasmon. The Drude's model describes the frequency at which this collective oscillation occurs as the bulk plasma oscillation frequency (ω_p) (Equation 6).

$$\omega_p = \sqrt{\frac{N_h e^2}{\epsilon_0 m_h}} \quad (6)$$

Where N_h represents the mobile electrons (holes) density, e is the charge of the electron, m_h is the electron (hole) effective mass ϵ_0 is the dielectric permittivity of vacuum.

When metals are in nanometres range, such as in NPs with a size comparable to a wavelength, and all the NPs are illuminated with the appropriate wavelength to produce resonance, then a LSPR is produced. LSPR in NPs depends on several factors, such as the metal type, the size and shape of the NP, and the surrounding media. Every metal has a complex dielectric function (ϵ_m) that depends on the wavelength λ according to the Equation 7:

$$\epsilon_m(\lambda) = \epsilon_{\text{real}}(\lambda) + \epsilon_{\text{im}}(\lambda) \quad (7)$$

The real part of the dielectric function determines the frequency at which electron oscillation resonance occurs, while the imaginary part incorporates the broadening and absorptive dissipation of this resonance due to damping and dephasing of the electron oscillations. In this context, the dielectric constants for NPs at different wavelengths are assumed to match those of bulk metals. For most metals, excluding some noble and alkali ones, ϵ_{im} is typically very large, which suppresses the excitation of surface plasmons in the visible region. Meanwhile, ϵ_{real} , which correlates with the ability to absorb light, is negative for alkali and noble

metals. In non-noble metals, interband transitions contribute positively to ϵ_{real} , hindering the excitation of surface plasmon modes in small metal spheres. For example, both Au and Ag NPs exhibit intense LSPR, but the Ag LSPR exhibits markedly greater intensity compared to Au. This difference can be attributed to the disparities in their ϵ_{im} . Ag possesses a notably smaller ϵ_{im} , consequently experiencing lower dissipative losses than Au. This translates to a higher scattering quantum yield for Ag NPs, indicating a greater proportion of incident light being scattered as opposed to absorbed.

Furthermore, the narrower bandwidth and sharper LSPR peak observed in Ag NPs can be ascribed to the combination of a smaller ϵ_{im} and a steeper slope (reflecting a greater magnitude) of the real component of the dielectric function ϵ_{real} . This leads to a more restricted range of resonant frequencies, resulting in a sharper peak in the LSPR spectrum. Consequently, Ag NPs surpass Au in terms of their light-scattering efficiency within the vis-NIR region [105]. The size of the NPs affects their optical and electronic properties due to the quantum confinement of the conduction electrons, thus absorption wavelength is directly proportional to the radius of NPs, so as the NP size decreases the LSPR wavelength also decreases (Equation 8):

$$\gamma = \gamma_{\infty} + \frac{A v_f}{R} \quad (8)$$

where γ_{∞} is the scattering rate of the free electrons in bulk metal, A is a constant, v_f is the Fermi velocity of the electrons, and R is the radius of the NPs. The shape of the NPs can change the surface polarization, and therefore LSPR at desired wavelengths can be achieved by synthesising NPs with different morphologies. The relationship between the LSPR shift and shape of particles can be established as in Equation 9:

$$\Delta\lambda = \frac{\Delta N}{2N} \lambda_{\text{sp}} \sqrt{\epsilon_{\infty} + \left(\frac{1-\eta}{\eta}\right) \epsilon_{\text{medium}}} \quad (9)$$

Where N is the electron density in the metals, λ_{sp} is the SPR wavelength for metals, ϵ_{∞} is the high-frequency contribution to the metal dielectric function, ϵ_{medium} is the dielectric constant of the medium, and η is the particle shape factor.

In addition to the dipolar mode (**Figure 11**), which is the most commonly observed and studied mode, higher-order modes such as the quadrupole and octupole LSPR can also occur in plasmonic NPs. These higher-order modes involve more complex charge distributions within the NP, resulting in resonances at higher energies compared to the dipolar mode. The quadrupole LSPR involves the collective oscillation of electrons along two perpendicular axes, leading to a quadrupolar charge distribution within the nanoparticle. Similarly, the octupole LSPR involves the collective oscillation of electrons along three perpendicular axes, resulting in an octupolar charge distribution. Because of the more complex charge distributions involved in higher-order modes, their energies typically increase with increasing multipole order. This means that quadrupole LSPR occurs at higher energies than dipole LSPR, and octupole LSPR occurs at even higher energies than quadrupole LSPR (**Figure 12**) [106]. Moreover, LSPR is sensitive to the surrounding medium and its absorption wavelength maximum

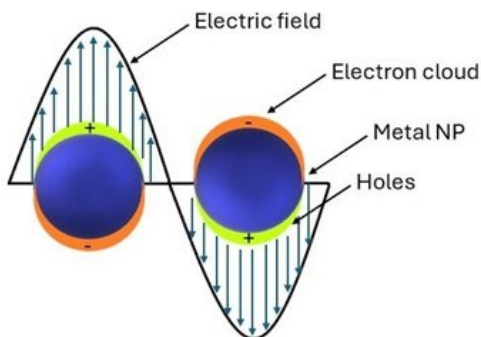


Figure 11. Illustration of the dipolar surface plasmon resonance, with the collective oscillation of the conduction band electrons due to an incident electric field.

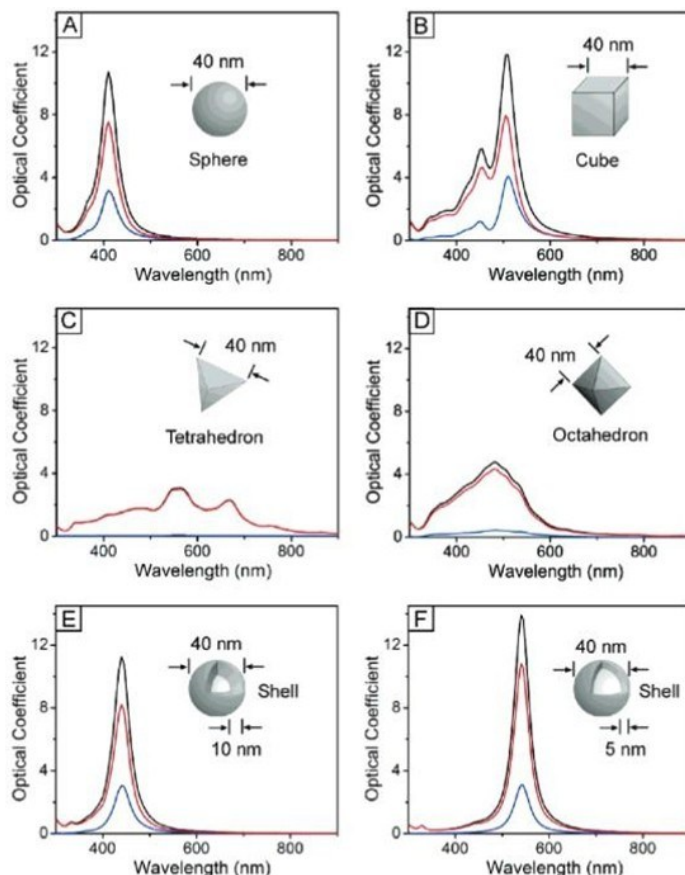


Figure 12. Calculated UV-vis extinction (black), absorption (red), and scattering (blue) spectra of Ag nanostructures, illustrating the effect of a nanostructure's shape on its spectral characteristics. An isotropic sphere (A) exhibit spectra with a single resonance peak. Anisotropic cubes (B), tetrahedra (C), and octahedra (D) exhibit spectra with multiple, red-shifted resonance peaks. The resonance frequency of a sphere red-shifts if it is made hollow (E), with further red-shift for thinner shell walls (F). Reproduced with permission from reference [106] Copyright 2006 American Chemical Society.

λ_{max} changes as the dielectric constant ϵ or refractive index n of the medium is changed. The LSPR frequency can then also be shifted by varying the environment (stabilizer, functionalization or solvent molecules) and as a consequence the dielectric constant of the NPs-environment system. The field induced by the conjunct of NPs and their medium can be written in the form of effective polarizability and dipole moment as given by Equation 10:

$$\rho = \epsilon_m \alpha E_0 \quad (10)$$

Where ρ is the effective dipole moment of the NP-medium system, E_0 is the incident electric field, α is the dipolar polarizability and ϵ_m is the dielectric constant of embedding media. When the NPs are coated with a dielectric material of thickness d and dielectric constant ϵ_d , then polarizability α is defined by Equation 11:

$$\alpha = 4\pi\epsilon_0(R+d)^3 \frac{\epsilon_d\epsilon_a - \epsilon_a\epsilon_b}{\epsilon_d\epsilon_a + 2\epsilon_m\epsilon_b} \quad (11)$$

Where a is the NP's radius and ϵ_a is the dielectric constant of the NP. Similarly, b is the total radius of the NP-medium system and ϵ_b is the dielectric constant of the NP-medium system. A red-shift in

absorption spectra is observed with the increase in the dielectric constant of the environment. The magnitude of the spectral shift $\Delta\lambda$ for NPs is described in Equation 12:

$$\Delta\lambda_{\max} = m\Delta n \left(1 - e^{-\frac{2d}{\ell d}} \right) \quad (12)$$

Where m is the bulk refractive-index response of the NPs, Δn is the change in the refractive index induced by the adsorbate, d is the effective adsorbate layer thickness, and ℓd is the characteristic electromagnetic field decay length. Thus, shell materials with a higher refractive index will lead to a larger red-shift with broadening of LSPR peaks.

4. Application of Metallic NPs

Metallic NPs, thanks to the huge variety of structures and composition, play a crucial role in various fields, from electronics to healthcare to agriculture and environmental remediation [93,107]. Some of these applications, where plasmonic and composite NPs are applied, are discussed below.

4.1. Healthcare

The healthcare sector includes a diverse array of needs and applications. A few applications where NPs have an impact are presented below.

4.1.1. Antibacterial activity and Antibiotic resistance

In recent years, significant efforts have been directed towards addressing the ever increasing problem of antibiotic resistance [108], whether by seeking alternatives or enhancing the efficacy of existing antibiotics through the integration of nanomaterials. Additionally, great efforts have been devoted to exploring methods to prevent bacterial proliferation on surfaces and biofilm formation. Ag NPs are undoubtedly the most extensively studied NPs for mitigating antibiotic resistance as their antibacterial properties have been known for centuries [109]. However, more recently also Cu and ZnO NPs have been investigated for their intrinsic antibacterial activity [110,111]. Ag and ZnO NPs have demonstrated synergistic effect with several antibiotics against a variety of bacteria through diverse modes of action, such as metal ions release, non-oxidative and oxidative stress [112–114]. Additionally, Ag, Cu, and ZnO NPs have shown the ability to synergize with conventional antibiotics and disrupt bacterial efflux pumps, a key mechanism involved in biofilm formation [115]. Research has concluded that Ag NPs can enhance the efficacy of antibiotics against pathogens commonly encountered in veterinary medicine, regardless of antibiotic resistance [116]. NPs with antibacterial properties can be also integrated in devices. Ag, Au, Cu, ZnO and TiO₂ have demonstrated to be able to increase the antibacterial properties of chitosan when applied as wound dressing to avoid bacterial contamination and infections, and also by enhancing healing through the regulation of re-epithelialisation and inflammation [117]. Moreover, medical implants, catheters, and healthcare fabrics can be integrated with metallic antibacterial NPs to mitigate infection risks and bacterial transmission in

healthcare setting [118]. Tri-elemental AgCuMg NPs, despite being in the early stages of development, have demonstrated antibacterial activity against both gram-positive and gram negative bacteria when integrated into coatings [119]. Similarly, hydrogel coatings loaded with Cu NPs have exhibited pronounced antibacterial properties and adhered well to stainless steel medical equipment [120]. Recent research has emphasised the significance of surface topographies in conferring antibacterial properties. Different morphologies found in nature are being studied for their potential to further enhance antibacterial surfaces. The combination of antibacterial surface topographies and antibacterial NPs holds promise in reducing infections and controlling their spread [121,122]. The primary drawbacks of using NPs for their antibacterial properties might be a limited stability on the NPs and an excessively fast ions release from the particle. Composite NPs, such as Ag@mesoporous SiO₂ NPs, have the potential to overcome these disadvantages and confer superior properties compared to bare NPs. Thanks to the accessible and porous network of the protective SiO₂ layer, the encapsulated nanocrystals can release antibacterial Ag ions in a steadier and continuous manner [123], furthermore the SiO₂ shell can help to prevent aggregation and increase the NPs solubility. The mesoporous channels can then be additionally used for encapsulation of active molecules, such as antibiotics, to treat antibiotic resistant infections [124] or to accelerate the healing of infected wounds [125].

4.1.2. Imaging, diagnosis and cancer treatment

Plasmonic NPs, due to their unique optical properties, find applications in diagnostics, particularly for biomedical imaging of tissues and for the detection of cancer cells. The composition and the shape of the NPs are adjustable, thus making it possible to tune the NPs based on the desired scattering [126]. For instance, NPs that scatter light in the near-infrared (NIR) range allow for a high-resolution deep tissue bioimaging [127]. Furthermore, NPs can be functionalized with antibodies, aptamers, or peptides to confer specific cellular binding features, thereby enhancing imaging precision and detection sensitivity. The functionalized NPs can be assembled to obtain a "detection kit" for a series of different diseases [128,129]. Coating NPs with a mesoporous SiO₂ shell can increase the biocompatibility and the cell up-take of the nanomaterial making them suitable for potential in vivo imaging applications. For example, biomolecule - conjugated Au nanorods encapsulated in a mesoporous SiO₂ shell were specifically taken up by cancer cells *in vitro* [130]. Mesoporous SiO₂ can also be modified with functional groups and conjugated with biomolecules for specific labelling of cells. Photoacoustic imaging, an emerging technique in biomedical imaging, can be significantly enhanced through the use of plasmonic NPs as contrast agents. In this imaging modality, a short laser pulse is directed onto the tissue under examination, causing rapid thermal expansion and the generation of ultrasound waves. These waves are then captured by ultrasound transducers and translated into high-resolution images. Au NPs are favoured in this application due to their biocompatibility, ease of functionalization, and adjustable LSPR. Current research efforts are concentrated on optimizing NPs for photoacoustic imaging within the second NIR window (1000 - 1700 nm). This spectral range

offers reduced background noise and scattering in biological tissues, thereby facilitating clearer and more precise imaging [131]. Other than diagnosis, plasmonic NPs can also find application in therapy. When plasmonic NPs are irradiated at their resonance wavelength they will generate a temperature rise in their proximity. This effect has found application in photothermal therapy, that is a non invasive technique utilized for cancer treatment. Plasmonic NPs, and particularly Au NPs are excellent candidates for this therapy due to the easy cell take-up, easy functionalization for specific cells targeting, and easy LSPR tuning. For photothermal therapy, the 650 - 900 nm range is preferred for application because minimal skin and tissue absorption allows light to penetrate deep into tissues in a non-invasive manner. The generated heat can induce thermal damage to cancer cells, leading to their destruction and vascular disruption that consist in damaging the tumour's blood vessels, compromising the tumour's viability [132,133]. Composite NPs can also add extra functionalities to the phototherapeutic treatment such as the delivery of a drug encapsulated in a mesoporous structure [134,135] or in a hollow plasmonic structure [136]. The generated heat can act as a trigger for the release of an encapsulated drug, while profiting of the augmented cell membrane permeability due to higher temperature [93,137]. Additional functionalities, such as magnetic properties, can enhance the NPs targeting of cancer cells through magnetic-guided photothermal therapy [138].

4.2. Sensing

4.2.1. Plasmonic sensing

NPs are particularly sensitive to their surrounding environment and this property made them to find application as plasmonic sensors for ex-situ analysis. Plasmonic sensors can detect subtle changes reflected in modifications of the LSPR of the colloidal system. Due to their outstanding optical properties, Au and Ag NPs are mostly used for this type of sensing. Analytes can be detected in a *yes/no* fashion or also quantified as a consequence of different phenomena [139]:

- *Analyte detection based on aggregation of NPs:* the addition of analytes to the colloidal system can cause a decrease the inter-particle distance of the NPs leading to their aggregation and to a change in shape and position of the LSPR. The amount of analyte can be estimated with spectroscopic or colorimetric techniques [140,141].
- *Analyte detection based on oxidation of NPs:* in the presence of analyte NPs can undergo oxidation, thus the number of metallic NPs in solution will decrease leading to a change in the colour of the solution and of the LSPR intensity. The analyte quantity can then be estimated observing the changes at a specific wavelength [142].
- *Analyte detection based on dimensional change of NPs:* certain analytes can cause a change the morphology/dimension of the NPs. In this case, a change in the LSPR profile will be observed, some bands will be quenched while others might appear [143].

Plasmonic NPs applied in sensing might undergo extra functionalization with different molecules such as oligonucleotides, proteins and amino acids, organic polymers, and organic

compounds. Functionalized plasmonic NPs can provide specificity towards target analytes, allowing for higher selectivity and sensitivity in the detection process. Functionalization can enhance the stability and dispersibility of the NPs and further regulate the detection mechanisms [144].

4.2.2. Surface-Enhanced Raman Spectroscopy

Raman scattering is inherently a weak phenomenon up to ten orders of magnitude weaker than fluorescence [145], but it offers high specificity. The combination of Raman's specificity with the plasmonic field enhancement provided by plasmonic nanostructures, known as Surface-Enhanced Raman Spectroscopy (SERS), first observed in 1973 for pyridine adsorbed on a roughened silver electrode [146], can exponentially increase the intensity of Raman signals, enabling the detection of even single molecules of analyte [107,147,148]. Molecules adsorb onto the surface of metallic nanostructures, and when laser light is directed onto the substrates, it interacts with the LSPR of the NPs, resulting in a significant enhancement of the Raman scattering signal. SERS can be performed either in a colloidal solution or, more commonly, with the solution containing the analyte deposited on a surface previously functionalized with metallic NPs. The shape, size, and arrangement of the NPs greatly influence the enhancement of the Raman signal. Au and Ag NPs, both in pure and alloyed compositions, are the most commonly used. A greater field enhancement occurs when NPs exhibit tips, cavities, and overall anisotropic morphology [145]. Additionally, the disposition and inter-particle distances of the NPs determine the effectiveness of a SERS substrate [147], in this case SiO₂ shells can be employed to further regulate the arrangement and distances between NPs. Mesoporous SiO₂ is generally preferred, as its channels permit the diffusion of analyte molecules to come into proximity with the metallic surface. Moreover, the shell can serve a protective function, increasing the stability of the NPs and preventing possible aggregations and reshaping phenomena [93].

4.2.3. Surface-Enhanced Fluorescence

The phenomenon of fluorescence is widely used in sensing, thanks to its fastness, reliability and high sensitivity. However, the major limitation is constituted by the quantum yield and fluorescence lifetime of the fluorophore [149]. Similarly to SERS, plasmonic near-field enhancement can enhance the light emission by fluorophores located in close vicinity of metallic nanostructures, in a phenomenon known as Surface-Enhanced Fluorescence (SEF). A crucial parameter for SEF is the distance between the NPs and the analyte molecules. Fluorophores can not, in fact, be in contact with the metallic surface, otherwise their emission will be quenched, while a distance of a few nm will dramatically increase it. As spacers, either thin metal oxide layer or SiO₂ layers can be used, the latter being more flexible regarding the possibility of synthesising shells with different thicknesses. SiO₂ shells can be also further functionalized to increase the detection of specific analytes [93]. Alloyed NPs with tunable composition and SiO₂ shells with multiple functionalisation's, combining the scattering of NPs and the SEF effect, can provide a platform for multiplex-detection allowing for the detection of numerous targets within the same

sample, thus providing a comprehensive view of the system [107,150].

4.3. Catalysis

Catalytic processes have brought significant advancements in research and technology, enabling the production of fertilizers, plastics, chemicals, and environmental remediation, such as the catalytic removal of pollutants from car exhausts.

4.3.1. Metallic NPs in catalysis

Metallic NPs have shown potential in the field of catalysis, as their properties are different from the one of their bulk counterparts and the reduction of the size brings an increment in the high surface to volume ratio, and thus active sites for the catalysis to happen. The composition, size and shape of the NPs are of great importance in the determination of the catalytic properties of the nanocrystals. For example, Au bulk surfaces are known to be inert, but in 1987 it was discovered that Au NPs were effective for low temperature CO oxidation [151,152]. Decreasing the size of the NPs can lead to an increase in the number of corner atoms and edges, that will lead to a higher degree of surface unsaturation. This variation can impact the bond strength of reaction intermediates with the catalyst, while corners and edges also offer diverse surface configurations for molecules to adsorb [153–155]. An increase in edges and corners is also obtainable with the synthesis of anisotropic NPs. Shape, that means which crystal facets are exposed to the reagents, has a significant importance on the catalytic properties of the NPs. Specifically, NPs that present tips and edges, considered active sites for the catalytic reaction, usually display better properties. When NPs have a quasi-spherical shape and exhibit only (111) low energy facets, their catalytic efficiency is usually lower compared to NPs of the same metal but with different morphologies that expose higher

energy (100) facets [156]. Furthermore, shape can also determine the selectivity of a reaction, for example in the benzene hydrogenation over cubic and cuboctahedral Pt NPs. Cuboctahedral NPs, characterized by the presence of (111) facets, lead to the formation of cyclohexane and cyclohexene, while cubic NPs, characterized by the presence of (100) facets, only lead to the formation of cyclohexane [152,157].

4.3.2. Composite NPs in catalysis

Composite NPs can have a prominent role in catalysis thanks to the great variety of combinations of structures and materials. Metallic NPs, for instance, can be encapsulated within various materials and with different architectures such as core@shell and yolk@shell configurations, and supported by diverse substrates including MOFs, carbon, and dendrimers (**Figure 13**) [158]. The encapsulation of single catalytic NPs in a core@shell structure can offer several advantages, such as adding extra stabilization and protection and prolonging the life of the catalyser. Multicore core@shell NPs or non coated NPs can in fact face aggregation of the cores both in colloidal solution or during high temperature catalytic processes. An aggregation will inevitably bring to a loss of catalytic sites and consequently a decrease in the catalytic efficiency [159]. The yolk@shell architecture, often referred to as nanoreactor in the catalysis field, offers additional advantages compared to the core@shell structure. As the core is able to freely move inside the protective shell, there is more surface area, and thus more catalytic sites available [160]. Encapsulated structures can furthermore manifest a greater selectivity. The pores' size, either in nanoreactors or supports architectures [161], can be finely tuned to act as a molecular sieve and regulate molecular diffusion [158]. Extra functionalities can also be added to the surface of metallic NPs to improve the catalytic reaction rates [162].

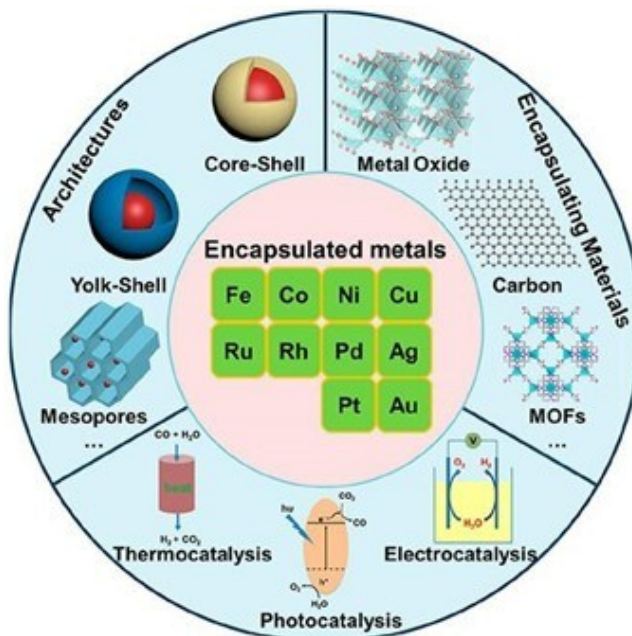


Figure 13. Encapsulated metal NPs with different architectures for catalytic applications. Reproduced with permission from reference [158] Copyright 2020 American Chemical Society.

Composite bimetallic NPs have emerged as a promising class of catalysts, offering unique properties and enhanced catalytic performance compared to their monometallic counterparts. By combining two different metals within the same NP, bimetallic NPs can exhibit synergistic effects, where the properties of the individual metals are combined and amplified, leading to improved catalytic activity and selectivity [163]. Bimetallic NPs can exhibit features on their surface such as migration, segregation, isolation of single atoms, surface enrichment, leading to the formation of structures with enhanced catalytic activity [164]. Pd based PdZn and PdPt bimetallic NPs, due to an increase of defects in the NPs structure and a change the electronic properties of the catalyst (ligand effect), demonstrated superior properties when compared to the Pd monometallic counterpart in the selective hydrogenation of dehydrolinalool [165]. PtAu NPs showed excellent properties in the reduction of 4-nitrophenol. The authors believe that the alloying of Pt and Au induces a strong synergistic effect that increase the catalytic activity, compared to pure Pt and pure Au NPs, by altering the electronic structure and the preferential adsorption of oxygen [166]. Ni@Pt NPs exhibited more than twice the catalytic activity of Pt NPs synthesized using the same method. ORR experiments demonstrated a significant enhancement in the activity of Ni@Pt catalysts compared to Pt alone. This increase in catalytic activity is attributed to alterations in geometric and/or electronic properties, which can influence the binding energy of oxygen and the adsorption of bisulfate anions [167].

4.3.3. Photocatalytic applications

Plasmonic metal NPs, either monometallic or bimetallic, due to their peculiar optical properties can be successfully employed in photocatalytic processes. The photocatalysts employed for a diverse range of chemical reactions under UV-visible light, are predominantly semiconductors. In such systems, semiconductors absorb photons, generating high-energy charge carriers (electron-hole pairs) within the semiconductor material. These charge carriers then dissociate and migrate to catalytically active sites situated at the semiconductor/liquid interface, where they facilitate various chemical transformations [168]. The most frequently utilized semiconductor is TiO₂. Because of its large band gap (3.0 - 3.2 eV), TiO₂ primarily absorbs light in the near UV region (<400 nm), which constitutes only a small portion of solar radiation (approximately 5%) [169]. Plasmonic NPs and semiconductors have emerged as a feasible combination to harvest a higher range of the solar spectrum. When deposited on TiO₂, a Schottky barrier will form at the interface between NPs and TiO₂, thus facilitating the electron-hole pairs separation and consequently enhancing the lacking photocatalytic activity of semiconductor materials under visible light [170].

AgAu NPs on TiO₂ have been used to degrade phenol in aqueous solution under visible light with more efficiency than Au NPs on TiO₂ [171]. The authors propose that the enhanced activity is attributed to electron transfer mechanisms. The presence of bimetallic NPs impedes charge recombination on Au NPs by facilitating electron transfer to Ag, known for its electron accepting abilities, and subsequently to the TiO₂ conduction band, facilitating the oxidation of phenol molecules by O₂ to form benzoquinone on

the AgAu surface, while keeping it in a reduced state. AuPd NPs on TiO₂ were used to demonstrate that the relative composition and the structure of the bimetallic NPs have influence on the photochemical H₂ evolution from ethanol aqueous solution. Core@shell Au@Pd bimetallic NPs showed the highest activity and NPs with a higher Pd content showed enhanced photoactivity, attributed to the fact that a thicker Pd shell supposedly shields photogenerated electrons from the recombination with holes [172]. Monometallic NPs deposited on TiO₂ were also utilized in water splitting and H₂ generation. Au NPs have successfully produced H₂ generation under visible light illumination, several experiments demonstrated the importance of different parameter such as the phase of the TiO₂ [173], and the size of the Au NPs [174]. Other than Au NPs, also monometallic Ag NPs [175] and Cu NPs [176] have been used for the same catalytic reaction. Cu NPs constitute a valid alternative to the rarer and more valuable Au and Ag.

Photocatalysis mediated by plasmonic NPs has proven an excellent tool in the field of environmental remediation. Several studies highlighted the potential degradation of pollutants either by NPs in solution or supported on TiO₂. Molecules such as methylene blue, rhodamine B, phenol are often chose as model for pollutants. Bio-synthesised CuO NPs [177], Ag NPs [178], degraded methylene blue and crystal violet in solution under sunlight. Supported NPs offer easier handling, recovery and the combination effect of the semiconductor support. Ag and Au NPs on mesoporous TiO₂ were tested for the degradation, as water pollutant models, of the azo dyes (congo red, methyl orange, acid orange 10, and remazol red) under solar and visible light irradiations. Both NPs improved the performance of TiO₂ with the Au NPs appearing to be the most promising candidates [179]. Photocatalysis can also be applied in the degradation of a class of rapidly emerging indoor pollutants known as volatile organic compounds (VOCs), of which examples are formaldehyde, acetaldehyde, methanol, ethylene, toluene.

Au supported on TiO₂ can degrade formaldehyde in air and under visible light. For the oxidation to happen the moisture present in the air has a decisive effect and visible light seems to accelerate the rate-determining steps of the reaction, leading to an overall possible degradation process for this VOC in ambient conditions [180]. Au@TiO₂ core@shell and yolk@shell structures demonstrated photocatalytic activity for the oxidation of gaseous toluene under visible light illumination. The yolk@shell architecture, with greater surface area and numerous mesoporous channels that can enhance the absorption of VOCs and provide more active sites, proved to have the best activity and reusability [181]. Photocatalysis offers a potential solution to the energy crisis and rising CO₂ emissions caused by human activities. CO₂ is a highly stable molecule and conventional thermolysis methods used for CO₂ degradation require harsh conditions and thus high energy consumption [169]. CO₂ photocatalytic conversion aided by plasmonic NPs is a hugely studied process and promising result have already been reported in the obtention of valuable products such as CH₄, CH₃OH, and C₂H₅OH. NPs of different compositions supported on different TiO₂ structures have been tested for CO₂ reduction. Au NPs and Pt NPs on TiO₂ nanofibers surpassed the catalytic properties of the semiconductor alone thanks to the synergistic effect of the two types of metals, Au LSPR effect that improves charge separation in

the semiconductor and Pt NPs which serve as electron-sink and active site. Ag NPs loaded on TiO₂ nanotube arrays promote a more efficient CO₂ reduction thanks to the LSPRS properties of Ag. When exposed to light hot electrons will be generated on the Ag NPs which are subsequently injected into the conduction band of TiO₂, promoting efficient charge separation and hindering electron-hole recombination. Furthermore, the localized near-field effect induced by the Ag NPs accelerates the transport of electrons within the nanotubes, leading to improved charge carrier transport efficiency [182]. Highly crystalline Cu NPs deposited onto anatase TiO₂ were found to convert CO₂ into CO while suppressing the competitive mechanism of hydrogen evolution. This study also highlighted the importance of the careful consideration of the most beneficial amount of NPs, as an excessive quantity of Cu demonstrated to be undesirable for the reaction [183].

4.4. Energy

The transition from fossil to alternative fuels is crucial for a sustainable and healthy future for our planet. Plasmonic NPs have gained attention as a possible solution to increase the exploitation of solar energy [184]. Plasmonic NPs, thanks to their absorption and scattering properties, can be efficiently integrated in solar light harvesting devices to maximize their harvesting capability [93].

Au NPs, with a size of approximately 45 nm, were incorporated into organic photovoltaic solar cells (OPVs) based on polymers. The resulting plasmonic enhanced OPV device exhibited a significant increase in light absorption due to localized field enhancement induced by LSPR, without compromising the device's electrical properties [185]. A further improvement in VOCs performance can be promoted by utilizing NPs protected by a SiO₂ shell. Core@shell particles can, in fact, be partially embedded on the active layer interface of the device. The SiO₂ shell serves many purposes such as maintaining the desired inter-particle distance and preventing changes in the morphology of the particle [186]. Similarly, NPs can be incorporated in dye-sensitized solar cells (DSSC). These cells utilize the light-absorbing properties of dyes, particularly in the visible range, to sensitize a metal oxide film, usually TiO₂. To take advantage of the absorption properties of plasmonic NPs, the use of anisotropic NPs and mixtures of different morphologies has been explored. For example, studies have shown that Au@Ag₂S nanorods [187] and mixtures of Ag NPs [188] can enhance the efficiency of DSSC devices due to their broader light absorption range compared to the commonly used spherical NPs.

5. Conclusions

Metallic NPs provide an exceptional platform for exploring the relationship between synthesis, structure, and functionality. As discussed throughout this review, the choice of synthetic strategy, whether top-down, bottom-up, direct, or seed-mediated, determines the resulting morphology, stability, and performance of the material. A solid understanding of the principles governing nucleation, growth, and stabilization is therefore essential to design NPs with properties tailored to specific functions. Beyond their

synthesis, the optical, catalytic, and biological behaviours of metallic NPs illustrate how nanoscale features influence macroscopic performance. Their LSPRs enable powerful sensing techniques, while catalytic activity can be precisely adjusted through control of size, shape, and composition. Applications across healthcare, energy, and environmental monitoring demonstrate both their versatility and growing relevance.

By combining historical developments, theoretical insights, and practical considerations, this introductory review seeks to clarify the connections between synthetic methods and resulting properties. The intention is not only to describe the main strategies available but also to encourage critical analysis, creative experimental design, and continued exploration of improved synthetic approaches.

Acknowledgements

S.N. thanks the FCT/MCTEC (Fundação para a Ciência e Tecnologia and Ministério da Ciência, Tecnologia e Ensino Superior) Portugal for her doctoral grant associated with the Chemistry PhD program (SFRH/BD/144618/2019). This work was supported by the Associate Laboratory for Green Chemistry LAQV which is financed by national funds from Fundação para a Ciência e Tecnologia and Ministério da Ciência, Tecnologia e Ensino Superior (FCT/MCTES) through the the project UID/50006/2023 of the Associate Laboratory for Green Chemistry - LAQV REQUIMTE, details here: <https://laqv.requimte.pt/a/74-funding>. PROTEOMASS Scientific Society (Portugal) is also acknowledged by the funding provided through the General Funding Grants 2024-2025.

References

- [1] J. Ogden, *Interdiscip. Sci. Rev.* 17 (1992) 261–270. DOI: 10.1179/030801892791925475
- [2] S. Medici, M. Peana, V.M. Nurchi, M.A. Zoroddu, *J. Med. Chem.* 62 (2019) 5923–5943. DOI: 10.1021/acs.jmedchem.8b01439
- [3] D.A. Scott, W. Bray, *Platin. Met. Rev.* 24 (1980) 147–157. DOI: 10.1595/003214080X244147157
- [4] M. Radetzki, *Resour. Policy* 34 (2009) 176–184. DOI: 10.1016/j.resourpol.2009.03.003
- [5] J. Pérez-Arantegui, J. Molera, A. Larrea, T. Pradell, M. Vendrell-Saz, I. Borgia, B.G. Brunetti, F. Cariatì, P. Fermo, M. Mellini, A. Sgamellotti, C. Viti, *J. Am. Ceram. Soc.* 84 (2001) 442–46. DOI: 10.1111/j.1151-2916.2001.tb00674.x
- [6] F. Antonii, *Panacea Aurea, Sive Tractatus Duo de Ipsius Auro Potabili, Ex Bibliopolio Frobeniano*, Hamburg, 1618.
- [7] J. Kunckel, *Nuetliche Observationes Oder Anmerkungen von Auro Und Argento Potabili*, Hamburg, 1676.

- [8] C. Chan, (2008). DOI: <https://www.sciencehistory.org/stories/magazine/from-nanotech-to-nanoscience/>
- [9] The Stained Glass Association of America, (2025). DOI: <https://stainedglass.org/learning-resources/history-stained-glass>
- [10] I. Freestone, N. Meeks, M. Sax, C. Higgitt, *Gold Bull.* 40 (2007) 270–277. DOI: 10.1007/BF03215599
- [11] R. November, R. February, *Philos. Trans. R. Soc. London* 147 (1857) 145–181. DOI: 10.1098/rstl.1857.0011
- [12] D. Thompson, *Gold Bull.* 40 (2007) 267–269. DOI: 10.1007/BF03215598
- [13] J. Turkevich, P.C. Stevenson, J. Hillier, *Discuss. Faraday Soc.* 11 (1951) 55. DOI: 10.1039/df9511100055
- [14] G. Mie, *Ann. Phys.* 330 (1908) 377–445. DOI: 10.1002/andp.19083300302
- [15] N. Abid, A.M. Khan, S. Shujait, K. Chaudhary, M. Ikram, M. Imran, J. Haider, M. Khan, Q. Khan, M. Maqbool, *Adv. Colloid Interface Sci.* 300 (2022) 102597. DOI: 10.1016/j.cis.2021.102597
- [16] P.G. Jamkhande, N.W. Ghule, A.H. Bamer, M.G. Kalaskar, *J. Drug Deliv. Sci. Technol.* 53 (2019) 101174. DOI: 10.1016/j.jddst.2019.101174
- [17] J. Polte, *CrystEngComm* 17 (2015) 6809–6830. DOI: 10.1039/C5CE01014D
- [18] N.T.K. Thanh, N. Maclean, S. Mahiddine, *Chem. Rev.* 114 (2014) 7610–7630. DOI: 10.1021/cr400544s
- [19] R. Becker, W. Döring, *Ann. Phys.* 416 (1935) 719–752. DOI: 10.1002/andp.19354160806
- [20] V.K. LaMer, R.H. Dinegar, *J. Am. Chem. Soc.* 72 (1950) 4847–4854. DOI: 10.1021/ja01167a001
- [21] W. Ostwald, *Zeitschrift Für Phys. Chemie* 34U (1900) 495–503. DOI: 10.1515/zpch-1900-3431
- [22] J.R. Shimpi, D.S. Sidhaye, B.L. V Prasad, *Langmuir* 33 (2017) 9491–9507. DOI: 10.1021/acs.langmuir.7b00193
- [23] M. José-Yacamán, C. Gutierrez-Wing, M. Miki, D.-Q. Yang, K.N. Piyakis, E. Sacher, *J. Phys. Chem. B* 109 (2005) 9703–9711. DOI: 10.1021/jp0509459
- [24] E.J.H. Lee, C. Ribeiro, E. Longo, E.R. Leite, *J. Phys. Chem. B* 109 (2005) 20842–20846. DOI: 10.1021/jp0532115
- [25] T.L. Moore, L. Rodriguez-Lorenzo, V. Hirsch, S. Balog, D. Urban, C. Jud, B. Rothen-Rutishauser, M. Lattuada, A. Petri-Fink, *Chem. Soc. Rev.* 44 (2015) 6287–6305. DOI: 10.1039/C4CS00487F
- [26] N. Shirtcliffe, U. Nickel, S. Schneider, *J. Colloid Interface Sci.* 211 (1999) 122–129. DOI: 10.1006/jcis.1998.5980
- [27] N.G. Bastús, F. Merkoçi, J. Piella, V. Puentes, *Chem. Mater.* 26 (2014) 2836–2846. DOI: 10.1021/cm500316k
- [28] Y. Ishida, T. Jirasupangkul, T. Yonezawa, *New J. Chem.* 39 (2015) 4214–4217. DOI: 10.1039/C5NJ00420A
- [29] N.R. Jana, L. Gearheart, C.J. Murphy, *J. Phys. Chem. B* 105 (2001) 4065–4067. DOI: 10.1021/jp0107964
- [30] Y. Sun, B. Gates, B. Mayers, Y. Xia, *Nano Lett.* 2 (2002) 165–168. DOI: 10.1021/nl010093y
- [31] N.G. Bastús, J. Comenge, V. Puentes, *Langmuir* 27 (2011) 11098–11105. DOI: 10.1021/la201938u
- [32] Y. Xia, K.D. Gilroy, H. Peng, X. Xia, *Angew. Chemie Int. Ed.* 56 (2017) 60–95. DOI: 10.1002/anie.201604731
- [33] L. Scarabelli, M. Sun, X. Zhuo, S. Yoo, J.E. Millstone, M.R. Jones, L.M. Liz-Marzán, *Chem. Rev.* 123 (2023) 3493–3542. DOI: 10.1021/acs.chemrev.3c00033
- [34] T.-H. Yang, J. Ahn, S. Shi, P. Wang, R. Gao, D. Qin, *Chem. Rev.* 121 (2021) 796–833. DOI: 10.1021/acs.chemrev.0c00940
- [35] A. Guerrero-Martínez, S. Barbosa, I. Pastoriza-Santos, L.M. Liz-Marzán, *Curr. Opin. Colloid Interface Sci.* 16 (2011) 118–127. DOI: 10.1016/j.cocis.2010.12.007
- [36] R. Jin, Y. Cao, C.A. Mirkin, K.L. Kelly, G.C. Schatz, J.G. Zheng, *Science* (80-.). 294 (2001) 1901–1903. DOI: 10.1126/science.1066541
- [37] S. Chen, D.L. Carroll, *Nano Lett.* 2 (2002) 1003–1007. DOI: 10.1021/nl025674h
- [38] Q. Zhang, Y. Hu, S. Guo, J. Goebel, Y. Yin, *Nano Lett.* 10 (2010) 5037–5042. DOI: 10.1021/nl1032233
- [39] C.H. Zhang, J. Zhu, J.J. Li, J.W. Zhao, *ACS Appl. Mater. Interfaces* 9 (2017) 17387–17398. DOI: 10.1021/acsami.7b04365
- [40] Y. Huang, A.R. Ferhan, Y. Gao, A. Dandapat, D.H. Kim, *Nanoscale* 6 (2014) 6496–6500. DOI: 10.1039/c4nr00834k
- [41] Y. Sun, B.T. Mayers, Y. Xia, *Nano Lett.* 2 (2002) 481–485. DOI: 10.1021/nl025531v
- [42] M.A. Mahmoud, M.A. El-Sayed, *Langmuir* 28 (2012) 4051–4059. DOI: 10.1021/la203982h

- [43] Z. Leng, X. Wu, X. Li, J. Li, N. Qian, L. Ji, D. Yang, H. Zhang, *Nanoscale Adv.* 4 (2022) 1158–1163. DOI: 10.1039/D1NA00842K
- [44] L. Lu, A. Kobayashi, K. Tawa, Y. Ozaki, *Chem. Mater.* 18 (2006) 4894–4901. DOI: 10.1021/cm0615875
- [45] Y.-H. Chen, H.-H. Hung, M.H. Huang, *J. Am. Chem. Soc.* 131 (2009) 9114–9121. DOI: 10.1021/ja903305d
- [46] Mahmoud, C.E. Tabor, M.A. El-Sayed, Y. Ding, Z.L. Wang, *J. Am. Chem. Soc.* 130 (2008) 4590–4591. DOI: 10.1021/ja710646t
- [47] Z. Fang, Y. Zhang, F. Du, X. Zhong, *Nano Res.* 1 (2008) 249–257. DOI: 10.1007/s12274-008-8029-0
- [48] J.D. Hoefelmeyer, K. Niesz, G.A. Somorjai, T.D. Tilley, *Nano Lett.* 5 (2005) 435–438. DOI: 10.1021/nl048100g
- [49] N.M. Ngo, H.-V. Tran, T.R. Lee, *ACS Appl. Nano Mater.* 5 (2022) 14051–14091. DOI: 10.1021/acsanm.2c02533
- [50] P. Senthil Kumar, I. Pastoriza-Santos, B. Rodríguez-González, F. Javier García de Abajo, L.M. Liz-Marzán, *Nanotechnology* 19 (2008) 015606. DOI: 10.1088/0957-4484/19/01/015606
- [51] M.B. Mohamed, K.Z. Ismail, S. Link, M.A. El-Sayed, *J. Phys. Chem. B* 102 (1998) 9370–9374. DOI: 10.1021/jp9831482
- [52] N.R. Jana, L. Gearheart, C.J. Murphy, *Adv. Mater.* 13 (2001) 1389–1393. DOI: 10.1002/1521-4095(200109)13:18<1389::AID-ADMA1389>3.0.CO;2-F
- [53] C.L. Nehl, H. Liao, J.H. Hafner, *Nano Lett.* 6 (2006) 683–688. DOI: 10.1021/nl052409y
- [54] S. Chen, Z.L. Wang, J. Ballato, S.H. Foulger, D.L. Carroll, *J. Am. Chem. Soc.* 125 (2003) 16186–16187. DOI: 10.1021/ja038927x
- [55] M. Schütz, D. Steinigeweg, M. Salehi, K. Kömpe, S. Schlücker, *Chem. Commun.* 47 (2011) 4216. DOI: 10.1039/c0cc05229a
- [56] H. Yuan, C.G. Khoury, H. Hwang, C.M. Wilson, G.A. Grant, T. Vo-Dinh, *Nanotechnology* 23 (2012) 075102. DOI: 10.1088/0957-4484/23/7/075102
- [57] S. Sasidharan, D. Bahadur, R. Srivastava, *RSC Adv.* 6 (2016) 84025–84034. DOI: 10.1039/C6RA11405A
- [58] I. Jung, S. Lee, S. Lee, J. Kim, S. Kwon, H. Kim, S. Park, *Chem. Rev.* 125 (2025) 7321–7388. DOI: 10.1021/acs.chemrev.4c00897
- [59] K. Loza, M. Heggen, M. Epple, *Adv. Funct. Mater.* 30 (2020). DOI: 10.1002/adfm.201909260
- [60] M. Sankar, N. Dimitratos, P.J. Miedziak, P.P. Wells, C.J. Kiely, G.J. Hutchings, *Chem. Soc. Rev.* 41 (2012) 8099. DOI: 10.1039/c2cs35296f
- [61] N. Blommaerts, H. Vanrompay, S. Nuti, S. Lenaerts, S. Bals, S.W. Verbruggen, *Small* 15 (2019) 1–8. DOI: 10.1002/smll.201902791
- [62] T. Fu, J. Fang, C. Wang, J. Zhao, *J. Mater. Chem. A* 4 (2016) 8803–8811. DOI: 10.1039/C6TA02202B
- [63] A.G.M. da Silva, T.S. Rodrigues, S.J. Haigh, P.H.C. Camargo, *Chem. Commun.* 53 (2017) 7135–7148. DOI: 10.1039/C7CC02352A
- [64] I. Lee, S.W. Han, K. Kim, *Chem. Commun.* 1 (2001) 1782–1783. DOI: 10.1039/b105437f
- [65] A.K. Verma, R.K. Soni, *Opt. Laser Technol.* 163 (2023) 109429. DOI: 10.1016/j.optlastec.2023.109429
- [66] M. Alheshibri, *Nanomaterials* 13 (2023) 2940. DOI: 10.3390/nano13222940
- [67] R. Intartaglia, G. Das, K. Bagga, A. Gopalakrishnan, A. Genovese, M. Povia, E. Di Fabrizio, R. Cingolani, A. Diaspro, F. Brandi, *Phys. Chem. Chem. Phys.* 15 (2013) 3075–3082. DOI: 10.1039/C2CP42656K
- [68] G. Li, Z. Tang, *Nanoscale* 6 (2014) 3995–4011. DOI: 10.1039/C3NR06787D
- [69] P. Rai, *Sustain. Energy Fuels* 3 (2019) 63–91. DOI: 10.1039/C8SE00336j
- [70] R.T. Tom, A.S. Nair, N. Singh, M. Aslam, C.L. Nagendra, R. Philip, K. Vijayamohan, T. Pradeep, *Langmuir* 19 (2003) 3439–3445. DOI: 10.1021/la0266435
- [71] S. Liu, M.D. Regulacio, S.Y. Tee, Y.W. Khin, C.P. Teng, L.D. Koh, G. Guan, M.-Y. Han, *Chem. Rec.* 16 (2016) 1965–1990. DOI: 10.1002/tcr.201600028
- [72] R. Ghosh Chaudhuri, S. Paria, *Chem. Rev.* 112 (2012) 2373–2433. DOI: 10.1021/cr100449n
- [73] R. Purbia, S. Paria, *Nanoscale* 7 (2015) 19789–19873. DOI: 10.1039/C5NR04729C
- [74] Z. Chen, Z.-M. Cui, F. Niu, L. Jiang, W.-G. Song, *Chem. Commun.* 46 (2010) 6524. DOI: 10.1039/c0cc01786h
- [75] Y. Dai, B. Lim, Y. Yang, C.M. Copley, W. Li, E.C. Cho, B. Grayson, P.T. Fanson, C.T. Campbell, Y. Sun, Y. Xia, *Angew. Chemie Int. Ed.* 49 (2010) 8165–8168. DOI: 10.1002/anie.201001839
- [76] M.-H. Jung, Y.J. Yun, M.-J. Chu, M.G. Kang, *Chem. – A Eur. J.*

- 19 (2013) 8543–8549. DOI: 10.1002/chem.201300834
- [77] L.M. Liz-Marzán, A.P. Philipse, J. Colloid Interface Sci. 176 (1995) 459–466. DOI: 10.1006/jcis.1995.9945
- [78] L.M. Liz-Marzán, M. Giersig, P. Mulvaney, Langmuir 12 (1996) 4329–4335. DOI: 10.1021/la9601871
- [79] W. Stöber, A. Fink, E. Bohn, J. Colloid Interface Sci. 26 (1968) 62–69. DOI: 10.1016/0021-9797(68)90272-5
- [80] T. Ung, L.M. Liz-Marzán, P. Mulvaney, Langmuir 14 (1998) 3740–3748. DOI: 10.1021/la980047m
- [81] T. Ung, L.M. Liz-Marzán, P. Mulvaney, J. Phys. Chem. B 103 (1999) 6770–6773. DOI: 10.1021/jp991111r
- [82] P. Mulvaney, M. Giersig, T. Ung, L.M. Liz-Marzán, Adv. Mater. 9 (1997) 570–575. DOI: 10.1002/adma.19970090712
- [83] C. Graf, D.L.J. Vossen, A. Imhof, A. van Blaaderen, Langmuir 19 (2003) 6693–6700. DOI: 10.1021/la0347859
- [84] C. Fernández-López, C. Mateo-Mateo, R.A. Álvarez-Puebla, J. Pérez-Juste, I. Pastoriza-Santos, L.M. Liz-Marzán, Langmuir 25 (2009) 13894–13899. DOI: 10.1021/la9016454
- [85] V. Salgueiriño-Maceira, M.A. Correa-Duarte, M. Spasova, L.M. Liz-Marzán, M. Farle, Adv. Funct. Mater. 16 (2006) 509–514. DOI: 10.1002/adfm.200500565
- [86] I. Pastoriza-Santos, J. Pérez-Juste, L.M. Liz-Marzán, Chem. Mater. 18 (2006) 2465–2467. DOI: 10.1021/cm060293g
- [87] O. Niitsoo, A. Couzis, J. Colloid Interface Sci. 354 (2011) 887–890. DOI: 10.1016/j.jcis.2010.11.013
- [88] C.T. Kresge, M.E. Leonowicz, W.J. Roth, J.C. Vartuli, J.S. Beck, Nature 359 (1992) 710–712. DOI: 10.1038/359710a0
- [89] R.I. Nooney, T. Dhanasekaran, Y. Chen, R. Josephs, A.E. Ostafin, Adv. Mater. 14 (2002) 529–532. DOI: 10.1002/1521-4095(20020404)14:7<529::AID-ADMA529>3.0.CO;2-H
- [90] P. Botella, A. Corma, M.T. Navarro, Chem. Mater. 19 (2007) 1979–1983. DOI: 10.1021/cm0629457
- [91] I. Gorelikov, N. Matsuura, Nano Lett. 8 (2008) 369–373. DOI: 10.1021/nl0727415
- [92] W.-C. Wu, J.B. Tracy, Chem. Mater. 27 (2015) 2888–2894. DOI: 10.1021/cm504764v
- [93] C. Hanske, M.N. Sanz-Ortiz, L.M. Liz-Marzán, Adv. Mater. 30 (2018) 1707003. DOI: 10.1002/adma.201707003
- [94] R.K. Kankala, H. Zhang, C.-G. Liu, K.R. Kanubaddi, C.-H. Lee, S.-B. Wang, W. Cui, H.A. Santos, K. Lin, A.-Z. Chen, Adv. Funct. Mater. 29 (2019) 1902652. DOI: 10.1002/adfm.201902652
- [95] P. Dikshit, J. Kumar, A. Das, S. Sadhu, S. Sharma, S. Singh, P. Gupta, B. Kim, Catalysts 11 (2021) 902. DOI: 10.3390/catal11080902
- [96] S. Ying, Z. Guan, P.C. Ofoegbu, P. Clubb, C. Rico, F. He, J. Hong, Environ. Technol. Innov. 26 (2022) 102336. DOI: 10.1016/j.eti.2022.102336
- [97] S. Swain, S.K. Barik, T. Behera, S.K. Nayak, S.K. Sahoo, S.S. Mishra, P. Swain, Bionanoscience 6 (2016) 205–213. DOI: 10.1007/s12668-016-0208-y
- [98] V. Dhand, L. Soumya, S. Bharadwaj, S. Chakra, D. Bhatt, B. Sreedhar, Mater. Sci. Eng. C 58 (2016) 36–43. DOI: 10.1016/j.msec.2015.08.018
- [99] N. González-Ballesteros, S. Prado-López, J.B. Rodríguez-González, M. Lastra, M.C. Rodríguez-Argüelles, Colloids Surfaces B Biointerfaces 153 (2017) 190–198. DOI: 10.1016/j.colsurfb.2017.02.020
- [100] A. Chahardoli, N. Karimi, A. Fattahi, Adv. Powder Technol. 29 (2018) 202–210. DOI: 10.1016/j.appt.2017.11.003
- [101] T. Ahmad, M. Irfan, S. Bhattacharjee, Procedia Eng. 148 (2016) 1396–1401. DOI: 10.1016/j.proeng.2016.06.558
- [102] M.D. Regulacio, D.-P. Yang, E. Ye, CrystEngComm 22 (2020) 399–411. DOI: 10.1039/C9CE01561B
- [103] R. Rodríguez-Oliveros, R. Paniagua-Domínguez, J.A. Sánchez-Gil, D. Macías, Nanospectroscopy 1 (2016). DOI: 10.1515/nansp-2015-0006
- [104] Y. Xia, D.J. Campbell, J. Chem. Educ. 84 (2007) 91. DOI: 10.1021/ed084p91
- [105] K.E. Fong, L.-Y.L. Yung, Nanoscale 5 (2013) 12043. DOI: 10.1039/c3nr02257a
- [106] B.J. Wiley, S.H. Im, Z.-Y. Li, J. McLellan, A. Siekkinen, Y. Xia, J. Phys. Chem. B 110 (2006) 15666–15675. DOI: 10.1021/jp0608628
- [107] L. Wang, M. Hasanzadeh Kafshgari, M. Meunier, Adv. Funct. Mater. 30 (2020) 2005400. DOI: 10.1002/adfm.202005400
- [108] Antimicrobial Resistance Collaborators. Global burden of bacterial antimicrobial resistance in 2019: a systematic analysis. Lancet. 2022 Feb 12;399(10325):629–655. doi: 10.1016/S0140-6736(21)02724-0. Epub 2022 Jan 19. Erratum in: Lancet. 2022 Oct 1;400(10358):1102. doi: 10.1016/S0140-6736(21)02653-2. PMID: 35065702; PMCID: PMC8841637.

- [109] L.P. Silva, A.P. Silveira, C.C. Bonatto, I.G. Reis, P. V Milreu, in: A. Ficaí, A.M. Grumezescu (Eds.), *Nanostructures Antimicrob. Ther.*, Elsevier, 2017, pp. 577–596. DOI: 10.1016/B978-0-323-46152-8.00026-3
- [110] E. Sánchez-López, D. Gomes, G. Esteruelas, L. Bonilla, A.L. Lopez-Machado, R. Galindo, A. Cano, M. Espina, M. Ettcheto, A. Camins, A.M. Silva, A. Durazzo, A. Santini, M.L. Garcia, E.B. Souto, *Nanomaterials* 10 (2020) 292. DOI: 10.3390/nano10020292
- [111] A.P. Ingle, N. Duran, M. Rai, *Appl. Microbiol. Biotechnol.* 98 (2014) 1001–1009. DOI: 10.1007/s00253-013-5422-8
- [112] A.S. Dove, D.I. Dzurny, W.R. Dees, N. Qin, C.C. Nunez Rodriguez, L.A. Alt, G.L. Ellward, J.A. Best, N.G. Rudawski, K. Fujii, D.M. Czyż, *Front. Microbiol.* 13 (2023). DOI: 10.3389/fmicb.2022.1064095
- [113] R. Vazquez-Muñoz, A. Meza-Villezas, P.G.J. Fournier, E. Soria-Castro, K. Juarez-Moreno, A.L. Gallego-Hernández, N. Bogdanchikova, R. Vazquez-Duhalt, A. Huerta-Saquero, *PLoS One* 14 (2019) e0224904. DOI: 10.1371/journal.pone.0224904
- [114] U.H. Abo-Shama, H. El-Gendy, W.S. Mousa, R.A. Hamouda, W.E. Yousuf, H.F. Hetta, E.E. Abdeen, *Infect. Drug Resist.* Volume 13 (2020) 351–362. DOI: 10.2147/IDR.S234425
- [115] D. Gupta, A. Singh, A.U. Khan, *Nanoscale Res. Lett.* 12 (2017) 454. DOI: 10.1186/s11671-017-2222-6
- [116] M. Smekalova, V. Aragon, A. Panacek, R. Prucek, R. Zboril, L. Kvitek, *Vet. J.* 209 (2016) 174–179. DOI: 10.1016/j.tvjl.2015.10.032
- [117] A. Mohandas, S. Deepthi, R. Biswas, R. Jayakumar, *Bioact. Mater.* 3 (2018) 267–277. DOI: 10.1016/j.bioactmat.2017.11.003
- [118] X. Yang, J. Hou, Y. Tian, J. Zhao, Q. Sun, S. Zhou, *Sci. China Technol. Sci.* 65 (2022) 1000–1010. DOI: 10.1007/s11431-021-1962-x
- [119] G. Benetti, E. Cavaliere, R. Brescia, S. Salassi, R. Ferrando, A. Vantomme, L. Pallecchi, S. Pollini, S. Boncompagni, B. Fortuni, M.J. Van Bael, F. Banfi, L. Gavioli, *Nanoscale* 11 (2019) 1626–1635. DOI: 10.1039/C8NR08375D
- [120] S. Cometa, R. Iatta, M.A. Ricci, C. Ferretti, E. De Giglio, J. *Bioact. Compat. Polym.* 28 (2013) 508–522. DOI: 10.1177/0883911513498960
- [121] A. Elbourne, R.J. Crawford, E.P. Ivanova, J. *Colloid Interface Sci.* 508 (2017) 603–616. DOI: 10.1016/j.jcis.2017.07.021
- [122] G. Mi, D. Shi, M. Wang, T.J. Webster, *Adv. Healthc. Mater.* 7 (2018) 1800103. DOI: 10.1002/adhm.201800103
- [123] M. Liong, B. France, K.A. Bradley, J.I. Zink, *Adv. Mater.* 21 (2009) 1684–1689. DOI: 10.1002/adma.200802646
- [124] Y. Wang, X. Ding, Y. Chen, M. Guo, Y. Zhang, X. Guo, H. Gu, *Biomaterials* 101 (2016) 207–216. DOI: 10.1016/j.biomaterials.2016.06.004
- [125] Q. Liu, Y. Zhang, J. Huang, Z. Xu, X. Li, J. Yang, H. Huang, S. Tang, Y. Chai, J. Lin, C. Yang, J. Liu, S. Lin, J. *Nanobiotechnology* 20 (2022) 386. DOI: 10.1186/s12951-022-01600-9
- [126] S. Patskovsky, E. Bergeron, D. Rioux, M. Simard, M. Meunier, *Analyst* 139 (2014) 5247–5253. DOI: 10.1039/C4AN01063A
- [127] H. Xu, Q. Li, L. Wang, Y. He, J. Shi, B. Tang, C. Fan, *Chem. Soc. Rev.* 43 (2014) 2650. DOI: 10.1039/c3cs60309a
- [128] K. Seekell, M.J. Crow, S. Marinakos, J. Ostrander, A. Chilkoti, W. Adam, J. *Biomed. Opt.* 16 (2011) 116003. DOI: 10.1117/1.3646529
- [129] A. Nsamela Matombi, M. Hasanzadeh Kafshgari, L. Wang, S. Patskovsky, D. Trudel, M. Meunier, *ACS Appl. Nano Mater.* 3 (2020) 4171–4177. DOI: 10.1021/acsanm.0c00376
- [130] Q. Zhan, J. Qian, X. Li, S. He, *Nanotechnology* 21 (2010) 055704. DOI: 10.1088/0957-4484/21/5/055704
- [131] Y. Mantri, J. V Jokerst, *ACS Nano* 14 (2020) 9408–9422. DOI: 10.1021/acsnano.0c05215
- [132] S.G. Alamdari, M. Amini, N. Jalilzadeh, B. Baradaran, R. Mohammadzadeh, A. Mokhtarzadeh, F. Oroojalian, J. *Control. Release* 349 (2022) 269–303. DOI: 10.1016/j.jconrel.2022.06.050
- [133] A.V.P. Kumar, S.K. Dubey, S. Tiwari, A. Puri, S. Hejmady, B. Gorain, P. Kesharwani, *Int. J. Pharm.* 606 (2021) 120848. DOI: 10.1016/j.ijpharm.2021.120848
- [134] Z. Liang, C. Cao, J. Gao, W. Cai, J. Li, D. Wu, Y. Kong, *ACS Appl. Nano Mater.* 5 (2022) 7440–7448. DOI: 10.1021/acsanm.2c01448
- [135] N.T. Ha Lien, A.D. Phan, B.T. Van Khanh, N.T. Thuy, N. Trong Nghia, H.T. My Nhung, T. Hong Nhung, D. Quang Hoa, V. Duong, N. Minh Hue, *ACS Omega* 5 (2020) 20231–20237. DOI: 10.1021/acsomega.0c01939
- [136] Z. Zhang, J. Wang, C. Chen, *Adv. Mater.* 25 (2013) 3869–3880. DOI: 10.1002/adma.201301890
- [137] Z. Lv, S. He, Y. Wang, X. Zhu, *Adv. Healthc. Mater.* 10 (2021) 2001806. DOI: 10.1002/adhm.202001806
- [138] A. Espinosa, J. Reguera, A. Curcio, Á. Muñoz-Noval, C. Kuttner, A. Van de Walle, L.M. Liz-Marzán, C. Wilhelm, *Small* 16

- (2020) 1904960. DOI: 10.1002/sml.201904960
- [139] A. Amirjani, D.F. Haghshenas, *Sensors Actuators B Chem.* 273 (2018) 1768–1779. DOI: 10.1016/j.snb.2018.07.089
- [140] A. Fernández-Lodeiro, J. Fernández-Lodeiro, C. Núñez, R. Bastida, J.L. Capelo, C. Lodeiro, *ChemistryOpen* 2 (2013) 200–207. DOI: 10.1002/open.201300023
- [141] J. Djafari, C. Marinho, T. Santos, G. Igrejas, C. Torres, J.L. Capelo, P. Poeta, C. Lodeiro, J. Fernández-Lodeiro, *ChemistryOpen* 5 (2016) 206–212. DOI: 10.1002/open.201600016
- [142] D. Sahu, N. Sarkar, G. Sahoo, P. Mohapatra, S.K. Swain, *Sensors Actuators B Chem.* 246 (2017) 96–107. DOI: 10.1016/j.snb.2017.01.038
- [143] S. Li, T. Wei, M. Tang, F. Chai, F. Qu, C. Wang, *Sensors Actuators B Chem.* 255 (2018) 1471–1481. DOI: 10.1016/j.snb.2017.08.159
- [144] A. Amirjani, E. Rahbarimehr, *Microchim. Acta* 188 (2021) 57. DOI: 10.1007/s00604-021-04714-3
- [145] A. Minopoli, A. Acunzo, B. Della Ventura, R. Velotta, *Adv. Mater. Interfaces* 9 (2022) 2101133. DOI: 10.1002/admi.202101133
- [146] M. Fleischmann, P.J. Hendra, A.J. McQuillan, *Chem. Phys. Lett.* 26 (1974) 163–166. DOI: 10.1016/0009-2614(74)85388-1
- [147] S. Schlücker, *Angew. Chemie Int. Ed.* 53 (2014) 4756–4795. DOI: 10.1002/anie.201205748
- [148] N. Akkilić, S. Geschwindner, F. Höök, *Biosens. Bioelectron.* 151 (2020) 111944. DOI: 10.1016/j.bios.2019.111944
- [149] A. Sultangazyev, R. Bukasov, *Sens. Bio-Sensing Res.* 30 (2020) 100382. DOI: 10.1016/j.sbsr.2020.100382
- [150] S. Tu, D. Rioux, J. Perreault, D. Brouard, M. Meunier, J. Phys. Chem. C 121 (2017) 8944–8951. DOI: 10.1021/acs.jpcc.6b11954
- [151] M. Haruta, T. Kobayashi, H. Sano, N. Yamada, *Chem. Lett.* 16 (1987) 405–408. DOI: 10.1246/cl.1987.405
- [152] A. Sági, T. Rajkumar, J. Kiss, Á. Kukovecz, Z. Kónya, G.A. Somorjai, *Catal. Letters* 151 (2021) 2153–2175. DOI: 10.1007/s10562-020-03477-5
- [153] K. An, G.A. Somorjai, *ChemCatChem* 4 (2012) 1512–1524. DOI: 10.1002/cctc.201200229
- [154] Z. Li, S. Ji, Y. Liu, X. Cao, S. Tian, Y. Chen, Z. Niu, Y. Li, *Chem. Rev.* 120 (2020) 623–682. DOI: 10.1021/acs.chemrev.9b00311
- [155] B. Hvolbæk, T.V.W. Janssens, B.S. Clausen, H. Falsig, C.H. Christensen, J.K. Nørskov, *Nano Today* 2 (2007) 14–18. DOI: 10.1016/S1748-0132(07)70113-5
- [156] S. Linic, P. Christopher, H. Xin, A. Marimuthu, *Acc. Chem. Res.* 46 (2013) 1890–1899. DOI: 10.1021/ar3002393
- [157] K.M. Bratlie, H. Lee, K. Komvopoulos, P. Yang, G.A. Somorjai, *Nano Lett.* 7 (2007) 3097–3101. DOI: 10.1021/nl0716000
- [158] C. Gao, F. Lyu, Y. Yin, *Chem. Rev.* 121 (2021) 834–881. DOI: 10.1021/acs.chemrev.0c00237
- [159] T. Zhang, H. Zhao, S. He, K. Liu, H. Liu, Y. Yin, C. Gao, *ACS Nano* 8 (2014) 7297–7304. DOI: 10.1021/nn502349k
- [160] S. Wang, M. Zhang, W. Zhang, *ACS Catal.* 1 (2011) 207–211. DOI: 10.1021/cs1000762
- [161] C. Wang, L. Wang, J. Zhang, H. Wang, J.P. Lewis, F.-S. Xiao, *J. Am. Chem. Soc.* 138 (2016) 7880–7883. DOI: 10.1021/jacs.6b04951
- [162] J. Lee, J.C. Park, J.U. Bang, H. Song, *Chem. Mater.* 20 (2008) 5839–5844. DOI: 10.1021/cm801149w
- [163] A.K. Singh, Q. Xu, *ChemCatChem* 5 (2013) 652–676. DOI: 10.1002/cctc.201200591
- [164] I. Mustieles Marin, J.M. Asensio, B. Chaudret, *ACS Nano* 15 (2021) 3550–3556. DOI: 10.1021/acs.nano.0c09744
- [165] L.M. Bronstein, D.M. Chernyshov, I.O. Volkov, M.G. Ezernitskaya, P.M. Valetsky, V.G. Matveeva, E.M. Sulman, *J. Catal.* 196 (2000) 302–314. DOI: 10.1006/jcat.2000.3039
- [166] J. Zhang, G. Chen, D. Guay, M. Chaker, D. Ma, *Nanoscale* 6 (2014) 2125–2130. DOI: 10.1039/C3NR04715F
- [167] F. Godínez-Salomón, M. Hallen-López, O. Solorza-Feria, *Int. J. Hydrogen Energy* 37 (2012) 14902–14910. DOI: 10.1016/j.ijhydene.2012.01.157
- [168] S. Linic, P. Christopher, D.B. Ingram, *Nat. Mater.* 10 (2011) 911–921. DOI: 10.1038/nmat3151
- [169] A. Kumar, P. Choudhary, A. Kumar, P.H.C. Camargo, V. Krishnan, *Small* 18 (2022) 2101638. DOI: 10.1002/sml.202101638
- [170] A. Zaleska-Medynska, M. Marchelek, M. Diak, E. Grabowska, *Adv. Colloid Interface Sci.* 229 (2016) 80–107. DOI: 10.1016/j.cis.2015.12.008
- [171] A. Zielińska-Jurek, E. Kowalska, J.W. Sobczak, W. Lisowski, B. Ohtani, A. Zaleska, *Appl. Catal. B Environ.* 101 (2011) 504–514. DOI: 10.1016/j.apcatb.2010.10.022

- [172] Y. Mizukoshi, K. Sato, T.J. Konno, N. Masahashi, *Appl. Catal. B Environ.* 94 (2010) 248–253. DOI: 10.1016/j.apcatb.2009.11.015
- [173] J.B. Priebe, J. Radnik, A.J.J. Lennox, M.-M. Pohl, M. Karnahl, D. Hollmann, K. Grabow, U. Bentrup, H. Junge, M. Beller, A. Brückner, *ACS Catal.* 5 (2015) 2137–2148. DOI: 10.1021/cs5018375
- [174] K. Qian, B.C. Sweeny, A.C. Johnston-Peck, W. Niu, J.O. Graham, J.S. DuChene, J. Qiu, Y.-C. Wang, M.H. Engelhard, D. Su, E.A. Stach, W.D. Wei, *J. Am. Chem. Soc.* 136 (2014) 9842–9845. DOI: 10.1021/ja504097v
- [175] H. Liang, Q. Meng, X. Wang, H. Zhang, J. Wang, *ACS Appl. Mater. Interfaces* 10 (2018) 14145–14152. DOI: 10.1021/acsami.8b00677
- [176] J. Nie, A.O.T. Patrocinio, S. Hamid, F. Sieland, J. Sann, S. Xia, D.W. Bahnemann, J. Schneider, *Phys. Chem. Chem. Phys.* 20 (2018) 5264–5273. DOI: 10.1039/C7CP07762A
- [177] S.K. Karuppannan, R. Ramalingam, S.B. Mohamed Khalith, M.J.H. Dowlath, G.I. Darul Raiyaan, K.D. Arunachalam, *Biocatal. Agric. Biotechnol.* 31 (2021) 101904. DOI: 10.1016/j.bcab.2020.101904
- [178] V. Seerangaraj, S. Sathiyavimal, S.N. Shankar, J.G.T. Nandagopal, P. Balashanmugam, F.A. Al-Misned, M. Shanmugavel, P. Senthilkumar, A. Pugazhendhi, *J. Environ. Chem. Eng.* 9 (2021) 105088. DOI: 10.1016/j.jece.2021.105088
- [179] S.A. Anjugam Vandarkuzhali, N. Pugazhenthiran, R. V Mangalaraja, P. Sathishkumar, B. Viswanathan, S. Anandan, *ACS Omega* 3 (2018) 9834–9845. DOI: 10.1021/acsomega.8b01322
- [180] X. Zhu, C. Jin, X.-S. Li, J.-L. Liu, Z.-G. Sun, C. Shi, X. Li, A.-M. Zhu, *ACS Catal.* 7 (2017) 6514–6524. DOI: 10.1021/acscatal.7b01658
- [181] Y. Wang, C. Yang, A. Chen, W. Pu, J. Gong, *Appl. Catal. B Environ.* 251 (2019) 57–65. DOI: 10.1016/j.apcatb.2019.03.056
- [182] J. Low, S. Qiu, D. Xu, C. Jiang, B. Cheng, *Appl. Surf. Sci.* 434 (2018) 423–432. DOI: 10.1016/j.apsusc.2017.10.194
- [183] Y. Lan, Y. Xie, J. Chen, Z. Hu, D. Cui, *Chem. Commun.* 55 (2019) 8068–8071. DOI: 10.1039/C9CC02891A
- [184] D.J. de Aberasturi, A.B. Serrano-Montes, L.M. Liz-Marzán, *Adv. Opt. Mater.* 3 (2015) 602–617. DOI: 10.1002/adom.201500053
- [185] J.-L. Wu, F.-C. Chen, Y.-S. Hsiao, F.-C. Chien, P. Chen, C.-H. Kuo, M.H. Huang, C.-S. Hsu, *ACS Nano* 5 (2011) 959–967. DOI: 10.1021/nn102295p
- [186] H. Choi, J.-P. Lee, S.-J. Ko, J.-W. Jung, H. Park, S. Yoo, O. Park, J.-R. Jeong, S. Park, J.Y. Kim, *Nano Lett.* 13 (2013) 2204–2208. DOI: 10.1021/nl400730z
- [187] S. Chang, Q. Li, X. Xiao, K.Y. Wong, T. Chen, *Energy Environ. Sci.* 5 (2012) 9444. DOI: 10.1039/c2ee22657j
- [188] R. Selvapriya, T. Abhijith, V. Ragavendran, V. Sasirekha, V.S. Reddy, J.M. Pearce, J. Mayandi, J. Alloys Compd. 894 (2022) 162339. DOI: 10.1016/j.jallcom.2021.162339